PHYSICAL REVIEW D **85,** 095025 (2012)

Hybrid fourth generation: Technicolor with top-seesaw mechanism

Hidenori S. Fukano* and Kimmo Tuominen†

Department of Physics, University of Jyväskylä, P.O. Box 35, FIN-40014 Jyväskylä, Finland
and Helsinki Institute of Physics, P.O. Box 64, FIN-00014 University of Helsinki, Finland

(Received 8 March 2012; published 31 May 2012)

We consider a model combining technicolor with the top-quark condensation. As a concrete model for technicolor, we use the minimal walking technicolor, and this will result in the appearance of a novel fourth generation whose leptons constitute a usual weak doublet while the QCD quarks are vectorlike singlets under the weak interactions. We carry out an analysis of the mass spectra and precision measurement constraints, and find the model viable. We contrast the model with present LHC data and discuss the future prospects.

DOI: 10.1103/PhysRevD.85.095025 PACS numbers: 12.60.Nz, 12.15.Ff

I. INTRODUCTION

The standard model (SM) of the elementary particle interactions is known to describe nature at the level of current observations. However, the SM is believed to be an incomplete theory, mainly, because we cannot explain the origin of the observed mass patterns of the matter fields, how many generations of the matter fields there are, or why there is an excess of matter over antimatter. There are many continuing efforts to work out these mysteries. One possible paradigm to explain the Higgs mechanism in the SM is by the strong coupling gauge theory dynamics. Along this line, technicolor (TC) was proposed [1] (for reviews, see [2–4]). Here, the electroweak symmetry breaking is due to the condensation of new matter fields called technifermions. Unfortunately, the old-fashioned but simple TC model based on the QCD-like gauge theory dynamics is incompatible with the electroweak precision data at the CERN LEP experiments [5]. Recently, we have introduced TC models that are compatible with the electroweak precision data [6,7]. In these TC models, technifermions transform in higher representation under the TC gauge group, and these models naturally lead to a walking behavior [8–11] of the technicolor coupling constant, thanks to a nontrivial infrared fixed point [12]. Many groups are studying via first principle calculations whether the nonperturbative gauge theory dynamics realize the proposed walking TC models [13–22]. Among several such walking TC models, one of the most promising candidates is the minimal walking technicolor (MWT) model. The matter content of MWT is two Dirac flavors of technifermions in the adjoint representation of the $SU(2)$ TC gauge group. When gauged under the electroweak interactions, one must cancel the Witten anomaly arising due to the odd number of techniquark doublets. In order to cancel this anomaly, a fourth generation of leptons is introduced into the model. With this particle content, the MWT model overcomes the obstacles arising from the electroweak precision tests [7]. It is interesting to note that perhaps anomaly cancellation in a more complete underlying theory may provide hints on the number of fermion generations [23].

For explaining various mass patterns of the known matter fields within a TC framework, a well-known approach is the extended TC (ETC) [24], in which the technifemions and the SM fermions are embedded into a larger gauge group ($\mathcal{G}_{\rm ETC}$). In ETC, after $\mathcal{G}_{\rm ETC}$ breaks down to the TC gauge group and the technifermion condensation is triggered by the TC gauge dynamics, the SM fermions obtain their masses via the massive ETC gauge bosons coupled with the technifermion condensates. If an ETC gauge group breaks sequentially, this model may explain the observed mass hierarchies of the SM fermions [25,26]. However, it is hard to explain a large top-quark mass, or more precisely, a top-bottom mass splitting. To address this particular issue, an alternative to ETC, the top-quark condensation model, was proposed in a form of the low-energy effective model [27–30]. This model was then completed by a topcolor model where, generically, a gauge group $SU(3)_{\rm QCD} \times U(1)_Y$ of the SM is typically extended to $\mathcal{G}_{\rm topC} = SU(3)_1 \times SU(3)_2 \times U(1)_{Y1} \times U(1)_{Y2}$ [31]. A model which combines TC/ETC and topcolor dynamics has been proposed [32], and several groups are pursuing model building along this line [33,34]. We can regard this type of model as a kind of low-scale TC [35–37], which may explain [38] the observed excess in the dijet invariant mass in the $W +$ jets events reported by the CDF Collaboration [39].

Recently, we have proposed a new possibility of a model, in which we combined the MWT model and the top-quark condensation [40]. This model is one of top-seesaw assisted TC models. The dynamics of top-quark condensation was taken to be similar as in the top-seesaw model [41–43]. A main new feature in our model with respect to earlier work is that in addition to explaining the mass patterns of the heavy SM fermions, it predicts a *hybrid* fourth generation. This means that the new leptons

*hidenori.f.sakuma@jyu.fi
†kimmo.i.tuominen@jyu.fi

transform as chiral fermions under the electroweak gauge group, but there are also new QCD quarks transforming as vectorlike fermions under this group.

Many aspects of a sequential fourth generation have been studied earlier [44]. For example, it has been shown that a sequential fourth generation can be accommodated by the electroweak precision data [45–50] and that the fourth generation quarks help to describe the current experimental data on CP violation and rare decays of B mesons better within the CKM paradigm [51–55]. The fourth-generation leptons have been discussed in various contexts [55–63]. Finally, it has been pointed out that the sequential fourth-generation model can trigger the electroweak symmetry breaking [64–67]. However, a nonsequential fourth generation is a less investigated option, which would arise naturally due to internal consistency of some other beyond the SM sector [23,68]. In the previous work [40], we have described the dynamics of this hybrid fourth-generation model and discussed several constraints coming from the experiments. In this paper, we will formulate the dynamics in the language of the effective theory which will allow us to compare the hybrid fourth-generation model with the current electroweak precision data and discuss also recent results from the LHC.

II. AN OVERVIEW OF THE MODEL AND DYNAMICS

We consider a model termed model B in [40], which combines the MWT model and top-quark condensation. The $SU(3)_c \times U(1)_Y$ of SM is in this model embedded into $\mathcal{G} = SU(3)_1 \times SU(3)_2 \times U(1)_{Y1} \times U(1)_{Y2}$. To see how the fourth-generation matter fields originate, consider the charge assignments of the technicolor fields: In MWT, the $SU(2)_L$ doublet technifermion ($\mathcal{Q}_L$) has $Y(\mathcal{Q}_L) = 1/6$ under the $U(1)_{Y2}$ gauge symmetry. Therefore, in order to cancel the Witten and gauge anomalies in the technicolor sector, we add one SM-like $SU(2)_L$ doublet of leptons. Moreover, in this model, the third-generation quarks are assumed to obtain their masses only by the seesaw mechanism after some condensations are triggered, but other quarks obtain their masses mainly by ETC interactions with the technifermion condensates. This mechanism is the same as in the top-quark seesaw model [41–43]. When we concentrate on the nontechnicolored new matter sector, there are one SM-like *chiral* lepton doublet and two *vectorlike* extra quarks. In this sense, we call it a *hybrid fourth-generation* model. A most minimal model consists of particles in Table I. Techniquarks of the MWT sector are denoted by $\mathcal{Q}_L$, $\mathcal{T}_R$, and $\mathcal{B}_R$, while the fourth-generation leptons, required to exist by the internal consistency of the MWT model, by $L_L^{(4)}$, $N_R^{(4)}$, and $E_R^{(4)}$. The usual SM fields are $Q^{(3)}/L^{(3)}$ denoting the third-generation and $Q^{(i)}/L^{(i)} (i = 1, 2)$ the first- and second-generation quarks/leptons; the "SM" in the charge assignments shown in the table represents the ordinary SM charge

TABLE I. Particle content and charge assignments of the model. $Q/L^{(1,2,3)}$ are the first-, second-, and third-generation quarks/leptons of the SM, and "SM" in the columns for quantum numbers stands for the ordinary SM charge. All fermions are represented in terms of the weak gauge eigenbasis.

Field	$SU(2)_{\mathrm{TC}}$	$SU(3)_1$	$SU(3)_2$	$SU(2)_L$	$U(1)_{Y1}$	$U(1)_{Y2}$
$\mathcal{Q}_L$	$\square\square$	1	1	2	0	1/6
$\mathcal{T}_R$	$\square\square$	1	1	1	0	2/3
$\mathcal{B}_R$	$\square\square$	1	1	1	0	−1/3
$L_L^{(4)}$	1	1	1	2	0	−1/2
$N_R^{(4)}$	1	1	1	1	0	0
$E_R^{(4)}$	1	1	1	1	0	−1
$Q_L^{(3)}$	1	3	1	2	1/6	0
$U_R^{(3)}$	1	1	3	1	0	2/3
$D_R^{(3)}$	1	1	3	1	0	−1/3
$L_L^{(3)}$	1	1	1	2	−1/2	0
$N_R^{(3)}$	1	1	1	1	0	0
$E_R^{(3)}$	1	1	1	1	−1	0
$U_L^{(4)}$	1	1	3	1	0	2/3
$U_R^{(4)}$	1	3	1	1	2/3	0
$D_L^{(4)}$	1	1	3	1	0	−1/3
$D_R^{(4)}$	1	3	1	1	−1/3	0
$Q^{(1,2)}$	1	1	3	SM	0	SM
$L^{(1,2)}$	1	1	1	SM	0	SM

values. Finally, the fields $U^{(4)}$ and $D^{(4)}$ are the fourth-generation QCD quarks transforming as vectorlike fermions under the electroweak (EW) gauge symmetry.

We consider the case that $SU(3)_1$ gauge coupling (h_1) is stronger than $SU(3)_2$ gauge coupling (h_2), i.e. the ratio $\cot\theta = h_1/h_2$ is larger than 1. Furthermore, we consider the $U(1)Y_1$ gauge coupling (h_1') to be stronger than the $U(1)Y_2$ gauge coupling (h_2'), which implies that the ratio $\cot\theta' = h_1'/h_2'$ is larger than 1. In the notation introduced above, the QCD coupling and hypercharge $U(1)_Y$ couplings are given by $g_{\mathrm{QCD}} = h_1 \sin\theta = h_2 \cos\theta$ and $g_Y = h_1' \sin\theta' = h_2' \cos\theta'$.

The breaking pattern $\mathcal{G} \to SU(3)_{\mathrm{QCD}} \times U(1)_Y$, assumed to occur at some energy $\mu \gg v_{\mathrm{weak}}$, leads to the appearance of 8 + 1 massive gauge bosons. The eight massive gauge bosons associated with the breaking of $SU(3)_1 \times SU(3)_2$ are called "colorons" and denoted with G'. The one massive gauge boson associated with the breaking of $U(1)_1 \times U(1)_2$ is denoted with Z'. Their masses are denoted, respectively, by $M_{G'}$ and $M_{Z'}$. At low energies, the interactions via colorons or Z' exchange lead to effective four-fermion interactions which we will write down explicitly below. Then, we can divide the model into three parts, which are the SM part, the MWT part, and the four-fermion interaction part. We concentrate on the four-fermion sector, and we neglect the first and second family

fermions for simplicity. We assume that the masses of all leptons in this model as well as the masses of light quarks are explained by some underlying ETC dynamics operating at much higher scales and we aim to explain dynamically only the mass patterns of the third and fourth quark generations.

The exchange of a heavy coloron, G', gives

$$\mathcal{L}^{4f}_{G'} = -\frac{4\pi\kappa_3}{2M^2_{G'}}\sum_{f,f'}^{SU(3)_1}(\bar{f}\gamma^\mu T^a f)(\bar{f}'\gamma_\mu T^a f') - \frac{4\pi}{2M^2_{G'}}\frac{\alpha^2_{\mathrm{QCD}}}{\kappa_3}\sum_{f,f'}^{SU(3)_2}(\bar{f}\gamma^\mu T^a f)(\bar{f}'\gamma_\mu T^a f'), \quad (1)$$

where $f \in SU(3)_i$ stands for $SU(3)_i$ charged fermions, while the exchange of a heavy Z' gives

$$\mathcal{L}^{4f}_{Z'} = -\frac{4\pi\kappa_1}{2M^2_{Z'}}\sum_{f,f'}(Y^{(f)}_1\bar{f}\gamma^\mu f)(Y^{(f')}_1\bar{f}'\gamma_\mu f') - \frac{4\pi}{2M^2_{Z'}}\frac{\alpha^2_Y}{\kappa_1}\sum_{f,f'}(Y^{(f)}_2\bar{f}\gamma^\mu f)(Y^{(f')}_2\bar{f}'\gamma_\mu f'), \quad (2)$$

where $Y^{(f)}_i$ shows hypercharge of f under the $U(1)_{Yi}$. Now, we concentrate on the parts derived from the more strongly interacting sectors $SU(3)_1$ and $U(1)_{Y1}$, and we assume that the contributions from the more weakly interacting gauge sector is negligible in comparison to the stronger sector contributions.

Applying Fiertz rearrangements to Eqs. (1) and (2), we obtain the four-fermion interactions which can be divided into two parts as

$$\mathcal{L}^{4f} = \mathcal{L}^{4f}_S + \mathcal{L}^{4f}_V, \quad (3)$$

where

$$\mathcal{L}^{4f}_S = [G_{3S} + \tfrac{1}{9}G_{1S}](\bar{U}^{(4)}_R Q^{(3)}_L)^2 + [G_{3S} - \tfrac{1}{18}G_{1S}] \times (\bar{D}^{(4)}_R Q^{(3)}_L)^2 + \tfrac{1}{2}G_{1S}(\bar{E}^{(3)}_R L^{(3)}_L)^2, \quad (4)$$

and

$$\mathcal{L}^{4f}_V = -[G_{3V} + \tfrac{1}{36}G_{1V}]\{(\bar{Q}^{(3)}_L\gamma_\mu Q^{(3)}_L)^2 + 2(\bar{U}^{(3)}_L\gamma^\mu D^{(3)}_L) \times (\bar{D}^{(3)}_L\gamma_\mu U^{(3)}_L)\} - [G_{3V} + \tfrac{4}{9}G_{1V}](\bar{U}^{(4)}_R\gamma_\mu U^{(4)}_R)^2 - [G_{3V} + \tfrac{1}{9}G_{1V}](\bar{D}^{(4)}_R\gamma_\mu D^{(4)}_R)^2 - 2[G_{3V} - \tfrac{2}{9}G_{1V}] \times (\bar{U}^{(4)}_R\gamma^\mu D^{(4)}_R)(\bar{D}^{(4)}_R\gamma_\mu U^{(4)}_R). \quad (5)$$

Here, the four-fermion couplings are given in terms of the parameters of the underlying theory as

$$G_{3S} = 4G_{3V} = \frac{8}{9}\frac{4\pi\kappa_3}{M^2_{G'}}, \qquad G_{1S} = 4G_{1V} = \frac{8\pi\kappa_1}{M^2_{Z'}}. \quad (6)$$

To analyze the formation of a dynamical condensate in this model, we concentrate on the interaction in Eq. (4); the interaction in Eq. (5) will contribute to the analysis of electroweak precision constraints. Regarding the interactions among third family leptons, it is enough to consider the scalar four-fermion interactions in Eq. (4) since we will treat them as massless in the calculation of electroweak precision constraints.

The analysis of the condensate formation is based on the conventional Nambu-Jona-Lasinio model treatment. Generally, a scalar four-fermion interaction implies the gap equation

$$\Sigma = \frac{2NG_S\Lambda^2}{(4\pi)^2}\Sigma\left[1 - \frac{\Sigma^2}{\Lambda^2}\ln\frac{\Lambda^2+\Sigma^2}{\Sigma^2}\right], \quad (7)$$

where Σ is the dynamical mass of fermions and $N = 3$ or 1 corresponding to the interaction derived from the $SU(3)$ or $U(1)$ gauge boson exchange, respectively. The ultraviolet scale below which the four fermions interactions are applicable is denoted by Λ, and we set $\Lambda = M_{G'} = M_{Z'}$ in this paper. To see how the critical coupling arises, we rewrite Eq. (7) as

$$\frac{\Sigma^3}{\Lambda^2}\ln\frac{\Lambda^2+\Sigma^2}{\Sigma^2} = \Sigma\left(\frac{1}{g_{\mathrm{crit}}} - \frac{1}{g}\right), \quad (8)$$

where $g \equiv 2N\Lambda^2G/(4\pi)^2$ and $g_{\mathrm{crit}} = 1$. One can easily see that the left-hand side in Eq. (8) is always positive, while the right-hand side can be positive only if $g > g_{\mathrm{crit}}$. Therefore, if $g < g_{\mathrm{crit}}$, the gap equation Eq. (7) does not have any dynamical mass solutions; it only has the trivial solution $\Sigma = 0$. On the other hand, if $g > g_{\mathrm{crit}}$ the gap equation has a nontrivial dynamical solution $\Sigma \neq 0$.

In the present model, from Eq. (4), the gap equations are given by

$$\Sigma_U = g^{(34)}_U\Sigma_U\left[1 - \frac{\Sigma^2_U}{\Lambda^2}\ln\frac{\Lambda^2+\Sigma^2_U}{\Sigma^2_U}\right], \qquad \Sigma_D = g^{(34)}_D\Sigma_D\left[1 - \frac{\Sigma^2_D}{\Lambda^2}\ln\frac{\Lambda^2+\Sigma^2_D}{\Sigma^2_D}\right], \quad (9)$$

where the dimensionless couplings are given by

$$g^{(34)}_U = \frac{3}{2\pi}\left[\frac{8}{9}\kappa_3 + \frac{2}{27}\kappa_1\right], \qquad g^{(34)}_D = \frac{3}{2\pi}\left[\frac{8}{9}\kappa_3 - \frac{1}{27}\kappa_1\right]. \quad (10)$$

The essential point, which leads to the desired seesaw mechanism for the heavy quark masses is, that in this model, after $\mathcal{G} \to SU(3)_{\mathrm{QCD}} \times U(1)_Y$ symmetry breaking, we are allowed to add SM gauge-invariant mass terms

$$\mathcal{L}^{0}_{\mathrm{mass}} = -M^{(43)}_U\bar{U}^{(4)}_L U^{(3)}_R - M^{(44)}_U\bar{U}^{(4)}_L U^{(4)}_R - M^{(43)}_D\bar{D}^{(4)}_L D^{(3)}_R - M^{(44)}_D\bar{D}^{(4)}_L D^{(4)}_R + \mathrm{H.c.} \quad (11)$$

Qualitatively, in order to realize the top-bottom mass splitting after the condensate formation, the parameters in Eq. (11) need to have some hierarchy; this is where the

seesaw mechanism enters. In our model, we find after fitting the physical masses of top and bottom quarks that $M_U^{(44)}/m_t \sim \Lambda/(1\ \mathrm{TeV})$, $M_U^{(43)}/m_t \sim \Lambda/(1\ \mathrm{TeV})$, $M_D^{(44)}/m_b \sim 50\Lambda/(1\ \mathrm{TeV})$, and $M_D^{(44)}/m_b \sim \Lambda/(1\ \mathrm{TeV})$, where Λ is the UV cutoff of the theory where the effective four-fermion interactions should be matched onto the massive gauge boson exchange in the underlying theory.

Since our approach is bottom-up model building, the origin of these terms is left unspecified. For example, the $M_{U/D}^{(44)}$ terms could arise from the vacuum expectation value of a scalar field in $(\bar{3}, 3)$ representation of $SU(3)_1 \times SU(3)_2$, while the $M_{U/D}^{(43)}$ terms could be induced by some underlying ETC interactions operating at yet higher scales in comparison to $M_{G'}$ and $M_{Z'}$ relevant for the breaking of $SU(3)_1 \times SU(3)_2$.

We also require that there is no condensation of third-generation leptons. This channel is controlled by the coupling

$$g_E^{(33)} = \frac{\Lambda^2}{8\pi^2} G_{1S} = \kappa_1. \tag{12}$$

In order to set a theoretical constraint for κ_3, κ_1, we consider the criticality conditions of the couplings $g_U^{(34)}$, $g_D^{(34)}$, and $g_E^{(33)}$ together with the position of the Landau pole of the $U(1)_{Y_1}$ coupling, which we assume to be more strongly coupled of the two $U(1)$ factors. For this purpose, we consider the renormalization group equation for the $U(1)_{Y_1}$ gauge coupling. At one loop, the renormalization group equation is given by

$$\frac{d\alpha_{Y1}}{d\ln\mu} = \frac{b_{Y1}}{2\pi}\alpha_{Y1}^2, \tag{13}$$

with $b_{Y1} = 40/9$. So, the running of α_{Y1} is

$$\frac{1}{\alpha_{Y1}(\mu)} - \frac{1}{\alpha_{Y1}(\Lambda_{\mathrm{UV}})} = \frac{b_{Y1}}{2\pi}\ln\frac{\Lambda_{\mathrm{UV}}}{\mu}, \tag{14}$$

where $\mu < \Lambda_{\mathrm{UV}}$. By definition, the Landau pole is reached at scale Λ_L, where $1/\alpha_{Y1}(\Lambda_L) = 0$. If we denote the scale of the symmetry breaking as $\Lambda < \Lambda_L$, then

$$\frac{1}{\alpha_{Y1}(\Lambda)} = \frac{b_{Y1}}{2\pi}\ln\frac{\Lambda_L}{\Lambda}. \tag{15}$$

Since the low-energy four-fermion coupling κ_1 is related to the gauge couplings of the $U(1)_{Y_1}$ and $U(1)_Y$ groups as $\kappa_1 = \alpha_{Y1} - \alpha_Y$, Eq. (15) allows one to determine κ_1 for given Λ_L/Λ.

The constraints on the parameter space (κ_3, κ_1) are shown in Fig. 1. To obtain the desired pattern of condensations, we need the criticality conditions $g_{U/D}^{(34)} > 1$ to hold. We want to avoid condensation of third-generation leptons, and hence we require that $g_E^{(33)} < 1$. These conditions result in the gap triangle shown in the figure. The dashed horizontal lines are determined by the constraint on the position of the Landau pole, Eq. (15).

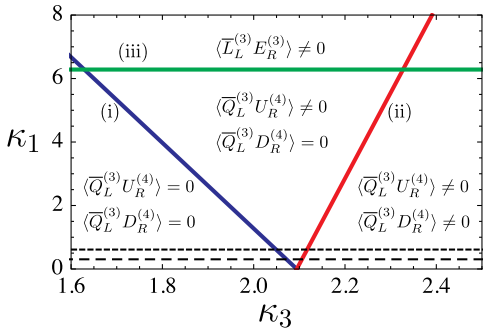

FIG. 1 (color online). The gap triangle for the present model. The region above (i) represents $\langle \bar{Q}_L^{(3)} U_R^{(4)} \rangle \neq 0$, the region below (ii) represents $\langle \bar{Q}_L^{(3)} D_R^{(4)} \rangle \neq 0$, and the region above (iii) represents $\langle \bar{L}_L^{(3)} E_R^{(3)} \rangle \neq 0$. The condensates of $Q_L^{(3)} - U_R^{(4)}$ and $Q_L^{(3)} - D_R^{(4)}$ form their condensates in an area which is to the right of (ii) and below (iii). The two dashed lines represent constraints from a position of the Landau pole, Eq. (15), for $\Lambda_L/\Lambda = 10$, 100 corresponding to the upper and lower lines.

III. EFFECTIVE LAGRANGIAN AND MASS SPECTRUM

In this section, we will apply the analysis of [43] to our model. We consider mixing of all generations, and assume the seesaw mechanism for the generation of fourth- and third-generation quark masses.

A. Gap equation in general

In order to consider the dynamical contributions from all quark generations, we diagonalize the quark mass matrix as follows:

$$U_{L/R}^{(\alpha)} = U_{\alpha\beta}^{L/R} u_{L/R}^{(\beta)}, \qquad D_{L/R}^{(\alpha)} = D_{\alpha\beta}^{L/R} d_{L/R}^{(\beta)}, \tag{16}$$

where $U_{\alpha\beta}^{L/R}$ and $D_{\alpha\beta}^{L/R}$ are unitary matices. Here, u, d are the fermion fields in the mass eigenbasis and the corresponding mass eigenvalues will be written as m_{ui} and m_{di}. In terms of the mass basis, the gap equations, Eq. (9), are

$$\Sigma_U = g_U^{(34)} \sum_{\alpha=1}^{4} \mathrm{Re}[U_{3\alpha}^L U_{4\alpha}^{R*}] m_{u\alpha}\left[1 - \frac{m_{u\alpha}^2}{\Lambda^2}\ln\frac{\Lambda^2 + m_{u\alpha}^2}{m_{u\alpha}^2}\right], \tag{17}$$

$$\Sigma_D = g_D^{(34)} \sum_{\alpha=1}^{4} \mathrm{Re}[D_{3\alpha}^L D_{4\alpha}^{R*}] m_{d\alpha}\left[1 - \frac{m_{d\alpha}^2}{\Lambda^2}\ln\frac{\Lambda^2 + m_{d\alpha}^2}{m_{d\alpha}^2}\right]. \tag{18}$$

B. Low-energy effective Lagrangian

Since the dynamical aspects of the top-seesaw sector are treated in the Nambu-Jona-Lasinio model, we can use the

fermion bubble sum approximation with $\mathcal{L}_S^{4f}$ in Eq. (4) [29,43] to obtain a low-energy effective Lagrangian valid for $\mu < \Lambda \simeq M_{G'} \simeq M_{Z'}$. In this section, we consider the low-energy effective Lagrangian for the top-seesaw sector in accordance with [43] and its mixing with the technicolor sector.

First, we introduce the auxiliary Higgs fields $\Phi_{1,2}^{(0)}$ as $\Phi_1^{(0)} \sim \bar{D}_R^{(4)} Q_L^{(3)}$ and $\Phi_2^{(0)} \sim \bar{U}_R^{(4)} Q_L^{(3)}$. Then, by using these auxiliary fields we can rewrite $\mathcal{L}_S^{4f}$ as

$$\mathcal{L}_{\mu=\Lambda}^{\text{Higgs}} = -\Lambda^2[|\Phi_1^{(0)}|^2 + |\Phi_2^{(0)}|^2] - [y_{10}\bar{Q}_L^{(3)}\Phi_1^{(0)} D_R^{(4)} + y_{20}\bar{Q}_L^{(3)}\tilde{\Phi}_2^{(0)} U_R^{(4)} + \text{H.c.}], \tag{19}$$

where $\tilde{\Phi}_i \equiv i\tau^2\Phi_i^*$, $y_{10} = [G_{3S} + (1/9)G_{1S}]\Lambda^2$, and $y_{20} = [G_{3S} - (1/18)G_{1S}]\Lambda^2$. Now, we parametrize $\Phi_i^{(0)}$ $(i = 1, 2)$ as

$$\Phi_i^{(0)} = \begin{pmatrix} \pi_{i0}^+ \\ \frac{1}{\sqrt{2}}[h_{i0}^0 - i\pi_{i0}^0] \end{pmatrix}. \tag{20}$$

So, in this picture, if the criticality condition $g_{U/D}^{(34)} > 1$ is satisfied, the fields $\Phi_i^{(0)}$ have nonzero vacuum expectation values, $\langle\Phi_i^{(0)}\rangle = (0, \langle h_{i0}^0\rangle/\sqrt{2})^T \neq 0$. This is obviously equivalent to $\Sigma_{U/D} \neq 0$. Now, one can easily see $\mathcal{L}_S^{4f} + \mathcal{L}_{\text{mass}}^0$ i.e. $\mathcal{L}_{\mu=\Lambda}^{\text{higgs}} + \mathcal{L}_{\text{mass}}^0$ has the Peccei-Quinn global $U(1)_A$ symmetry, under which each fermion transforms as [43]

$$\begin{aligned} &Q_L^{(3)} \to e^{-i\alpha} Q_L^{(3)}, \qquad U_R^{(3)} \to e^{i\alpha} U_R^{(3)}, \\ &D_R^{(3)} \to e^{i\alpha} D_R^{(3)}, \qquad U_{L/R}^{(4)} \to e^{i\alpha} U_{L/R}^{(4)}, \\ &D_{L/R}^{(4)} \to e^{i\alpha} D_{L/R}^{(4)}, \qquad \Phi_2^{(0)} \to e^{-2i\alpha}\Phi_2^{(0)}, \\ &\Phi_1^{(0)} \to e^{-2i\alpha}\Phi_1^{(0)}. \end{aligned} \tag{21}$$

If this $U(1)_A$ were an exact symmetry, its dynamical breaking by $\Sigma_{U/D} \neq 0$ would result in an appearance of a problematic massless Nambu-Goldstone boson. In the framework of topcolor model, this symmetry is explicitly broken by the topcolor instanton effect [32]. This can be represented by a four-fermion interaction of the form

$$\mathcal{L}_A = \frac{\xi h_1^2}{\Lambda^2}\epsilon^{ab}(\bar{U}_R^{(4)} Q_{L,a}^{(3)})(\bar{D}_R^{(4)} Q_{L,b}^{(3)}) + \text{H.c.}, \tag{22}$$

which can be rewritten using $\Phi_i^{(0)}$ as

$$\mathcal{L}_A = -\xi\Lambda^2[\epsilon^{ab}\Phi_{1,a}^{(0)}\Phi_{2,b}^{(0)}] - \xi\sqrt{4\pi\kappa_3}\{[\epsilon^{ab}\bar{Q}_{L,a}^{(3)}\Phi_{1,b}^{(0)}]D_R^{(4)} + [\epsilon^{ab}\bar{Q}_{L,a}^{(3)}\tilde{\Phi}_{2,b}^{(0)}]U_R^{(4)} + \text{H.c.}\}. \tag{23}$$

Here, ϵ^{ab} is the $SU(2)$ antisymmetric tensor and in Sec. V we will set $\xi = 10^{-3}$ in accordance with [43]. Of course, this topcolor instanton affects also gap equations. However, if $\xi \leq 10^{-3}$, this effect is negligible [43]. Therefore, the full Lagrangian at $\mu = \Lambda$ becomes $\mathcal{L}_\Lambda = \mathcal{L}_{\mu=\Lambda}^{\text{Higgs}} + \mathcal{L}_A$.

Using the fermion bubble sum approximation [29,43], the low-energy Lagrangian at $\mu < \lambda$ is

$$\mathcal{L}^{\text{Higgs}} = \mathcal{L}_{\text{kin}}^{\text{Higgs}}(\Phi_1, \Phi_2) - [y_1\bar{Q}_L^{(3)}\Phi_1 D_R^{(4)} + y_2\bar{Q}_L^{(3)}\tilde{\Phi}_2 U_R^{(4)} + \text{H.c.}] - V(\Phi_1, \Phi_2), \tag{24}$$

where the potential $V(\Phi_1, \Phi_2)$ is given by [43]

$$\begin{aligned} V(\Phi_1, \Phi_2) = {} & M_{11}^2|\Phi_1|^2 + M_{22}^2|\Phi_2|^2 - M_{12}^2[\Phi_1^\dagger\Phi_2 + \text{H.c.}] \\ & + \lambda_b(\Phi_1^\dagger\Phi_1)^2 + \lambda_t(\Phi_2^\dagger\Phi_2)^2 \\ & + \lambda_{tb}[(\Phi_1^\dagger\Phi_1)(\Phi_2^\dagger\Phi_2) - (\Phi_1^\dagger\Phi_2)(\Phi_2^\dagger\Phi_1)] \\ & + [\lambda_b'(\Phi_1^\dagger\Phi_1) + \lambda_t'(\Phi_2^\dagger\Phi_2)] \times [\Phi_1^\dagger\Phi_2 + \text{H.c.}]. \end{aligned} \tag{25}$$

Note that the Higgs quartic coupling terms in Eq. (25) correspond to similar terms in a generic two-Higgs-doublet model [69] after identifying the couplings in [69] as $\lambda_1 \to \lambda_b$, $\lambda_2 \to \lambda_t$, $\lambda_3 = -\lambda_4 = \lambda_{tb}$, $\lambda_5 = 0$, $\lambda_6 \to \lambda_b'$, $\lambda_7 \to \lambda_t'$.

Then, consider the low-energy effective theory of the pseudo-Nambu-Goldstone bosons (PNGBs) from the MWT described by the chiral Lagrangian based on the $G/H = SU(4)/SO(4)$ [70]. We decompose the nonlinear sigma model field $U(x)$ for $G_{\text{global}}/H_{\text{global}}$ as

$$\begin{aligned} U_{\text{TC}}(x) &= \xi_{\text{TC}}(x) \cdot E \cdot \xi_{\text{TC}}^T(x), \\ \xi(x)_{\text{TC}} &= \exp\left[\frac{i\Pi_{\text{TC}}(x)}{f_{\text{TC}}}\right], \end{aligned} \tag{26}$$

where $\Pi_{\text{TC}}(x) = \Pi^a(x)X^a$, $X^a \in \mathcal{G} - \mathcal{H}(a = 1, \cdots, 9)$ are NGB fields. Here, $\mathcal{G}$ and $\mathcal{H}$ denote the Lie algebra corresponding to G and H, respectively, and the decay constant for these NBGs is $f_{\text{TC}} = v_{\text{TC}}/\sqrt{2}$. For the concrete expressions of the generators X^a, see [70].

To simplify the notation, we will not explicate the variables x in what follows. The nonlinear sigma fields U_{TC}, ξ_{TC} transform as $U_{\text{TC}} \to gU_{\text{TC}}g^T$, $\xi_{\text{TC}} \to g\xi_{\text{TC}}g^T$ under G. The 4×4 matrix E is given by

$$E = \begin{pmatrix} 0_{2\times2} & 1_{2\times2} \\ 1_{2\times2} & 0_{2\times2} \end{pmatrix}, \tag{27}$$

which transforms $E \to gEg^T$ under G, and is invariant under H. The leading-order chiral Lagrangian is

$$\mathcal{L}_{\text{MWT}}^{\text{PNGBs}} = \frac{f_{\text{TC}}^2}{4}\,\text{tr}|D_\mu U|^2, \tag{28}$$

where the covariant derivative $D_\mu U_{\text{TC}}$ is given by

$$D_\mu U_{\text{TC}} = \partial_\mu U_{\text{TC}} - i[gW_\mu^a L^a + g'YB_\mu]U_{\text{TC}} - iU_{\text{TC}}[gW_\mu^a L^a + g'YB_\mu]^T. \tag{29}$$

Here, W^a_μ, B_μ are SM $SU(2)_L$ and $U(1)_Y$ gauge fields and g, g' their gauge couplings. The 4×4 matrices L^a and Y are given by

$$L^a = \begin{pmatrix} \sigma^a/2 & 0_{2\times 2} \\ 0_{2\times 2} & 0_{2\times 2} \end{pmatrix},$$
$$Y = \begin{pmatrix} y/2 & & & \\ & y/2 & & \\ & & -(1+y)/2 & \\ & & & -(y-1)/2 \end{pmatrix}, \tag{30}$$

here σ^a are the Pauli matrices, and $y/2$ is the hypercharge of the $SU(2)_L$ doublet technifermions.

Out of the nine NGBs ($\Pi_{\rm TC}$) in the MWT sector, three NGBs, denoted by $\pi_{\rm TC} = \pi^a_{\rm TC} X^a$ ($a = 1, 2, 3$), will mix with the dynamical Higgs bosons which arise as the composite objects of the 3rd and 4th family quarks. In order to consider this mixing, we first embed Φ_i in a form of 4×4 matrix as

$$\Sigma_i = \begin{pmatrix} 0 & 0 & \tilde{\Phi}_i & \Phi_i \\ 0 & 0 & & \\ {}^t\tilde{\Phi}_i & & 0 & 0 \\ {}^t\Phi_i & & 0 & 0 \end{pmatrix}, \tag{31}$$

where Φ_i ($i = 1, 2$) is as introduced in Eq. (25). We should note that Σ_i transforms under not full $G = SU(4)$ but only $SU(2)_L \times SU(2)_R \subset G$. Thus, the mixing between the top-seesaw sector and the MWT sector is [71]

$$V_M(U_{\rm TC}, \Sigma_1, \Sigma_2) = -c_1 v_1^2 \,{\rm tr}\left| \Sigma_1 - \frac{v_1}{\sqrt{2}} U_{\rm TC} \right|^2 - c_2 v_2^2 \,{\rm tr}\left| \Sigma_2 - \frac{v_2}{\sqrt{2}} U_{\rm TC} \right|^2, \tag{32}$$

where $c_{1,2} \sim \mathcal{O}(1)$ are dimensionless parameters.

The low-energy effective theory is now specified by Eqs. (24), (28), and (32); the full potential is given by adding (32) to (25). The stationary condition, $0 = \delta V/\delta\Phi|_{\langle\Phi_i\rangle}$, results in

$$0 = M_{11}^2 + \lambda_b v_1^2 + \tan\beta[-M_{12}^2 + \tfrac{3}{2}\lambda'_b v_1^2 + \tfrac{1}{2}\lambda'_t v_2^2], \tag{33}$$

$$0 = M_{22}^2 + \lambda_t v_2^2 + \cot\beta[-M_{12}^2 + \tfrac{1}{2}\lambda'_b v_1^2 + \tfrac{3}{2}\lambda'_t v_2^2]. \tag{34}$$

In addition to the vacuum expectation values v_1 and v_2 of the top-seesaw sector, we also have an electroweak symmetry breaking vacuum expectation value $v_{\rm TC}$ arising from MWT sector. These satisfy the constraint $v_1^2 + v_2^2 + v_{\rm TC}^2 = v_{\rm EW}^2$, where $v_{\rm EW} = 246$ (GeV). We define $\tan^2\phi = v_{\rm TC}^2/(v_1^2 + v_2^2)$, and then the above condition can be expressed as

$$v_1^2 + v_2^2 = v_{\rm EW}^2 \cdot \cos^2\phi. \tag{35}$$

To analyze the physical mass spectrum of the Higgs bosons in the present model, we simplify the parameter space by assuming that the states arising from the technicolor sector are heavy in comparison with the states arising from the topcolor sector. This means that we can obtain the physical spectrum by expanding Eq. (25) around $\langle\Phi_i\rangle = (0, v_i/\sqrt{2})^T$, and identifying the terms quadratic in the fields.

The quadratic terms of the Higgs boson fields are given by

$$\mathcal{L}_m^{\rm higgs} = -\frac{1}{2}\begin{pmatrix}\pi_1^0 & \pi_2^0\end{pmatrix}\mathcal{M}^2_\pi\begin{pmatrix}\pi_1^0 \\ \pi_2^0\end{pmatrix} - \begin{pmatrix}\pi_1^+ & \pi_2^+\end{pmatrix}\mathcal{M}^2_{\pi^\pm}\begin{pmatrix}\pi_1^- \\ \pi_2^-\end{pmatrix} - \frac{1}{2}\begin{pmatrix}h_1^0 & h_2^0\end{pmatrix}\mathcal{M}^2_h\begin{pmatrix}h_1^0 \\ h_2^0\end{pmatrix}. \tag{36}$$

Here, the mass matrix of CP-odd neutral Higgs boson fields (π_i^0), including the neutral top-pion of the topcolor model, is

$$\mathcal{M}^2_\pi = \left[M_{12}^2 - \frac{1}{2}\lambda'_b v_1^2 - \frac{1}{2}\lambda'_t v_2^2\right]\begin{pmatrix}\tan\beta & -1 \\ -1 & \cot\beta\end{pmatrix}. \tag{37}$$

The mass matrix of charged Higgs boson fields ($\pi_i^\pm$), which includes the charged top-pion, is

$$\mathcal{M}^2_{\pi^\pm} = \left[M_{12}^2 + \frac{1}{2}\lambda_{tb} v_1 v_2 - \frac{1}{2}\lambda'_b v_1^2 - \frac{1}{2}\lambda'_t v_2^2\right] \times \begin{pmatrix}\tan\beta & -1 \\ -1 & \cot\beta\end{pmatrix}, \tag{38}$$

and the mass matrix of CP-even neutral Higgs boson field (h_i^0) is

$$\mathcal{M}^2_h = \begin{pmatrix}2\lambda_1 v_1^2 & 0 \\ 0 & 2\lambda_2 v_2^2\end{pmatrix} + M_{12}^2\begin{pmatrix}\tan\beta & -1 \\ -1 & \cot\beta\end{pmatrix} + \frac{1}{2}v_1 v_2\begin{pmatrix}3\lambda'_b - \lambda'_t\tan^2\beta & 3\lambda'_b\cot\beta + 3\lambda'_t\tan\beta \\ 3\lambda'_b\cot\beta + 3\lambda'_t\tan\beta & 3\lambda'_t - \lambda'_b\cot^2\beta\end{pmatrix}, \tag{39}$$

where we define $\tan\beta \equiv v_2/v_1$. Among all Higgs bosons, three fields are absorbed as the longitudinal modes of the electroweak gauge bosons. The remaining three CP-odd Higgs boson fields, which we denote by A^0, $H^\pm$, and two CP-even Higgs bosons fields appear as the physical Higgs bosons in the low-energy spectrum. The CP-odd physical Higgs bosons and would-be Nambu-Goldstone bosons are related to the original fields of the seesaw sector as

$$\begin{pmatrix}G^0 \\ A^0\end{pmatrix} = \begin{pmatrix}\cos\beta & \sin\beta \\ -\sin\beta & \cos\beta\end{pmatrix}\begin{pmatrix}\pi_1^0 \\ \pi_2^0\end{pmatrix},$$
$$\begin{pmatrix}G^\pm \\ H^\pm\end{pmatrix} = \begin{pmatrix}\cos\beta & \sin\beta \\ -\sin\beta & \cos\beta\end{pmatrix}\begin{pmatrix}\pi_1^\pm \\ \pi_2^\pm\end{pmatrix}. \tag{40}$$

In this paper, we consider a scenario where the physical low-energy degrees of freedom arise dominantly from the

top-seesaw sector. Hence, we consider the NGBs $\pi_{\rm TC}$, arising from the MWT sector, to contribute to the mixing so that the NGBs absorbed by $W^{\pm}$, Z are represented by a linear combination of G^i and $\pi^i_{\rm TC}$ as

$$G_{\rm absorbed} = \cos\phi(\cos\beta\pi_1 + \sin\beta)\pi_2 + \sin\phi\,\pi_{\rm TC}. \quad (41)$$

The orthogonal linear combination $-\sin\phi(\cos\beta\pi_1 + \sin\beta)\pi_2 + \cos\phi\,\pi_{\rm TC}$ we take to be heavy and decoupled.

The masses of the physical CP-odd Higgs bosons are the nonzero eigenvalues of the matrices $\mathcal{M}^2_\pi$ and $\mathcal{M}^2_{\pi^\pm}$,

$$M^2_A = \frac{1}{\cos\beta\sin\beta}\left[M^2_{12} - \frac{1}{2}\lambda'_b v_1^2 - \frac{1}{2}\lambda'_t v_2^2\right], \quad (42)$$

$$M^2_{H^\pm} = M^2_A + \tfrac{1}{2}\lambda_{tb}[v_1\cos\beta + v_2\sin\beta]^2. \quad (43)$$

As to the CP-even Higgs bosons sector, we define $\tan 2\alpha \equiv 2[\mathcal{M}^2_h]_{12}/([\mathcal{M}^2_h]_{11} - [\mathcal{M}^2_h]_{22})$ with $-\pi/2 \le \alpha \le 0$. Then, the two mass eigenstates are represented by

$$\begin{pmatrix} H^0 \\ h^0 \end{pmatrix} = \begin{pmatrix} \cos\alpha & \sin\alpha \\ -\sin\alpha & \cos\alpha \end{pmatrix}\begin{pmatrix} h^0_1 \\ h^0_2 \end{pmatrix}, \quad (44)$$

and the corresponding mass eigenvalues are

$$M^2_{H^0} = \tfrac{1}{2}[[\mathcal{M}^2_h]_{11} + [\mathcal{M}^2_h]_{22} + \sqrt{([\mathcal{M}^2_h]_{11} - [\mathcal{M}^2_h]_{22})^2 + 4[\mathcal{M}^2_h]^2_{12}}], \quad (45)$$

$$M^2_{h^0} = \tfrac{1}{2}[[\mathcal{M}^2_h]_{11} + [\mathcal{M}^2_h]_{22} - \sqrt{([\mathcal{M}^2_h]_{11} - [\mathcal{M}^2_h]_{22})^2 + 4[\mathcal{M}^2_h]^2_{12}}]. \quad (46)$$

It is convenient to rewrite $[\mathcal{M}^2_h]_{11,22,12}$ with the help of M^2_A as

$$[\mathcal{M}^2_h]_{11} = 2\lambda_1 v_1^2 + 2\lambda'_b v_1 v_2 + M^2_A\sin^2\beta, \quad (47)$$

$$[\mathcal{M}^2_h]_{22} = 2\lambda_2 v_2^2 + 2\lambda'_t v_1 v_2 + M^2_A\cos^2\beta, \quad (48)$$

$$[\mathcal{M}^2_h]_{12} = M^2_A + 2v_1 v_2[\lambda'_b\cot\beta + \lambda'_t\tan\beta]. \quad (49)$$

We note that as $v^2_{\rm EW} = (246\ {\rm GeV})^2 = v^2_{\rm TC} + v_1^2 + v_2^2$ in our model and $\tan\phi \equiv v_{\rm TC}/\sqrt{v_1^2 + v_2^2}$, with $\tan\phi = 0$ we reproduce the results of the top-quark seesaw model in [43].

All these mass formulas are expressed in terms of the low-energy effective theory fields and parameters. However, by construction, the mass parameters $(M^2_{11,22,12})$ and quartic couplings $(\lambda_{b,t,tb}, \lambda'_{t,b})$ of the effective theory can be related to the parameters of the underlying ultraviolet theory by the direct computation of the two-point functions of the Higgs shown in Fig. 2(a), and four-point functions of the Higgs shown in Fig. 2(b).

Also, the low-energy fields Φ_i and couplings y_i in the low-energy Lagrangian are related to corresponding nonrenormalized fields $\Phi^{(0)}_i$ and couplings y_{i0} as

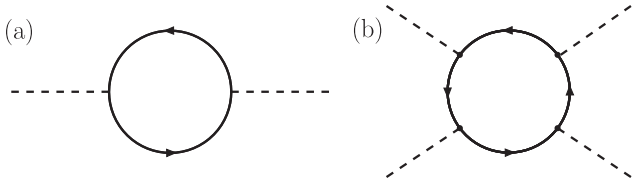

FIG. 2. Fermion contribution to the (a) two- and (b) four-point functions of the Higgs field. In these figures, solid lines and dashed lines correspond to fermion and Higgs, respectively.

$\Phi_i = Z^{1/2}_{\Phi_i}\Phi^{(0)}_i$ and $y_i = Z^{-1/2}_{\Phi_i} y_{i0}$. The wave function renormalization factors Z_{Φ_i} of the Higgs are evaluated by a direct computation of the two-point function of the Higgs in Fig. 2(a) as

$$Z_{\Phi_1} = \frac{3y^2_{10}}{16\pi^2}\left[\sum_{\alpha=1}^{4}|D^L_{\alpha3}|^2|D^R_{\alpha4}|^2\ln\frac{\Lambda^2 + m^2_{d\alpha}}{m^2_{d\alpha}} + \sum_{\alpha\neq\beta}|D^L_{\alpha3}|^2|D^R_{\beta4}|^2\ln\frac{\Lambda^2 + m^2_{d4}}{m^2_{d4}}\right], \quad (50)$$

$$Z_{\Phi_2} = \frac{3y^2_{20}}{16\pi^2}\left[\sum_{\alpha=1}^{4}|U^L_{\alpha3}|^2|U^R_{\alpha4}|^2\ln\frac{\Lambda^2 + m^2_{u\alpha}}{m^2_{u\alpha}} + \sum_{\alpha\neq\beta}|U^L_{\alpha3}|^2|U^R_{\beta4}|^2\ln\frac{\Lambda^2 + m^2_{u4}}{m^2_{u4}}\right]. \quad (51)$$

Here, we have assumed $m_{di} \ll m_{d4}$, $m_{ui} \ll m_{u4}$ for $i = 1, 2, 3$. Consequently, the component fields in Eq. (20) and their vacuum expectation values are also renormalized, e.g. $h^0_i = Z^{1/2}_{\Phi_i}h^0_{i0}$ and $v_i \equiv Z^{1/2}_{\Phi_i}\langle h^0_{i0}\rangle$. In terms of these variables, the dynamical fermion masses $\Sigma_{U/D}$ are represented as $\Sigma_{U(D)} = y_{2(1)}v_{2(1)}/\sqrt{2}$, i.e.

$$v_1^2 = \frac{3}{8\pi^2}\Sigma^2_D\left[\sum_{\alpha=1}^{4}|D^L_{\alpha3}|^2|D^R_{\alpha4}|^2\ln\frac{\Lambda^2 + m^2_{d\alpha}}{m^2_{d\alpha}} + \sum_{\alpha\neq\beta}|D^L_{\alpha3}|^2|D^R_{\beta4}|^2\ln\frac{\Lambda^2 + m^2_{d4}}{m^2_{d4}}\right], \quad (52)$$

$$v_2^2 = \frac{3}{8\pi^2}\Sigma^2_U\left[\sum_{\alpha=1}^{4}|U^L_{\alpha3}|^2|U^R_{\alpha4}|^2\ln\frac{\Lambda^2 + m^2_{u\alpha}}{m^2_{u\alpha}} + \sum_{\alpha\neq\beta}|U^L_{\alpha3}|^2|U^R_{\beta4}|^2\ln\frac{\Lambda^2 + m^2_{u4}}{m^2_{u4}}\right]. \quad (53)$$

As stated earlier, we may safely ignore the topcolor instanton effects for the gap equations.

The results of the calculation of the mass parameters and quadratic couplings in the low-energy theory are collected in Appendix B. To summarize the final results: The CP-odd Higgs boson A^0 obtains a dynamical mass given by Eq. (B1), the charged Higgs boson $H^\pm$ obtains a dynamical mass given by Eq. (B2) together with

Eqs. (B3)–(B5). Finally, the CP-even Higgs bosons H^0, h^0 ($M_{H^0} > M_{h^0}$) have dynamical masses given by Eqs. (45)–(49), together with Eqs. (B10)–(B12). These masses, as well as the fourth-generation quarks masses, $m_{t',b'}$, are determined for given values the parameters $\tan\beta$, $\tan\phi$, ξ, Λ with the criticality condition $g_{U/D} > 1$.

IV. OBLIQUE CORRECTIONS: S AND T PARAMETERS

Representing the self-energy of the electroweak gauge bosons as $\Pi^{\mu\nu}_{XY}(q^2) = g^{\mu\nu}\Pi_{XY}(q^2) + (q^\mu q^\nu\text{-term})$ where $XY = +-, 33, 3Y$, the Peskin-Takeuchi S, T parameters [5] are given by

$$S \equiv -16\pi \frac{\Pi_{3Y}(M_Z^2) - \Pi_{3Y}(0)}{M_Z^2}, \tag{54}$$

$$T \equiv \frac{4\pi}{M_Z^2 s_W^2 c_W^2}[\Pi_{+-}(0) - \Pi_{33}(0)]. \tag{55}$$

In the present model, the contributions from sectors beyond the SM are

$$S = S_{N,E} + S_{q4} + S_{\rm TC} + S_{\rm Higgs} + S_{G',Z'} + \Delta_S, \tag{56}$$

$$T = T_{N,E} + T_{q4} + T_{\rm TC} + T_{\rm Higgs} + T_{G',Z'} + \Delta_T, \tag{57}$$

where the first five terms on the right-hand side correspond to, from left to right, the contributions of the fourth leptons, the contributions of the fourth quarks, the contributions of the technicolor sector, the Higgs contributions and coloron and Z' contributions. The last term $\Delta_{S,T}$ is

$$\Delta_{S,T} = -\Delta_{S,T}(x_h^{\rm ref}) + \Delta_{S,T}(x_h^{\rm ours}). \tag{58}$$

This is the contribution from the light CP-even Higgs boson (h^0). The SM-Higgs contribution with $m_h^{\rm ref}$ is subtracted from the SM values $S_{\rm SM} = T_{\rm SM} = 0$. Here, $x_h \equiv m_h^2/M_Z^2$. In the present paper, we use $\Delta_{S,T}$ as defined in Appendix C of [72] [and denoted by H_S (H_T) for S (T) there].

A. Fourth-generation fermions contribution

The leading contributions to the S, T parameters from the fourth-generation leptons are [45,73]

$$S_{N,E} = \frac{1}{2\pi}[\psi_\nu(x_N) + \psi_e(x_E)], \tag{59}$$

$$T_{N,E} = \frac{1}{16\pi s_W^2 c_W^2}\theta_+(x_N, x_E), \tag{60}$$

where we do not consider a mixing between the fourth-generation leptons and the other three generation leptons, and we take the fourth-generation leptons heavy, $x_N \gg x_{\nu i}$ and $x_E \gg x_{ei}$ where $x_i \equiv m_i^2/M_W^2$, $i = 1, 2, 3$. On the other hand, since we consider the mixing for quark sectors, following [73], the one-loop contributions from the fourth-generation quarks sector are given by

$$\begin{aligned} S_{q4} = \frac{3}{2\pi}\Bigg[& (1 - |U_{44}^{(L)}|^2)\psi_u(x_{t'}) - \sum_{\alpha=1}^{3}|U_{4\alpha}^{(L)}|^2\psi_u(x_{u\alpha}) + (1 - |D_{44}^{(L)}|^2)\psi_d(x_{b'}) - \sum_{\alpha=1}^{3}|D_{4\alpha}^{(L)}|^2\psi_d(x_{d\alpha}) \\ & - \sum_{\alpha=1}^{3}|U_{4\alpha}^{(L)}|^2|U_{44}^{(L)}|^2\chi_+(x_{u\alpha}, x_{t'}) - \sum_{\alpha<\beta}(|U_{4\alpha}^{(L)}|^2|U_{4\beta}^{(L)}|^2 - 1)\chi_+(x_{u\alpha}, x_{u\beta}) \\ & - \sum_{\alpha=1}^{3}|D_{4\alpha}^{(L)}|^2|D_{44}^{(L)}|^2\chi_+(x_{d\alpha}, x_{b'}) - \sum_{\alpha<\beta}(|D_{4\alpha}^{(L)}|^2|D_{4\beta}^{(L)}|^2 - 1)\chi_+(x_{d\alpha}, x_{d\beta})\Bigg], \end{aligned} \tag{61}$$

$$\begin{aligned} T_{q4} = \frac{3}{16\pi s_W^2 c_W^2}\Bigg[& \sum_{\alpha=1}^{3}|U_{\alpha4}^{(L)}|^2|D_{\alpha4}^{(L)}|^2\theta_+(x_{t'}, x_{b'}) + \sum_{\alpha,\beta,\gamma=1}^{3}(|U_{\alpha\beta}^{(L)}|^2|D_{\alpha\gamma}^{(L)}|^2 - 1)\theta_+(x_{u\beta}, x_{d\gamma}) \\ & - \sum_{\alpha=1}^{3}|U_{4\alpha}^{(L)}|^2|U_{44}^{(L)}|^2\theta_+(x_{u\alpha}, x_{t'}) - \sum_{\alpha<\beta}(|U_{4\alpha}^{(L)}|^2|U_{4\beta}^{(L)}|^2 - 1)\theta_+(x_{u\alpha}, x_{u\beta}) \\ & - \sum_{\alpha=1}^{3}|D_{4\alpha}^{(L)}|^2|D_{44}^{(L)}|^2\theta_+(x_{d\alpha}, x_{b'}) - \sum_{\alpha<\beta}(|D_{4\alpha}^{(L)}|^2|D_{4\beta}^{(L)}|^2 - 1)\theta_+(x_{d\alpha}, x_{d\beta})\Bigg], \end{aligned} \tag{62}$$

where $x_{u\alpha} \equiv m_{u\alpha}^2/M_W^2$ and $x_{d\alpha} \equiv m_{d\alpha}^2/M_W^2$ and the functions $\psi_{\nu,e,u,d}(x)$ are given by

$$\psi_{+1/2}(Y, x) = \left(\frac{8Y}{3} + 2\right)x - \frac{2Y}{3}\ln x + \frac{(4Y+3)x + 2Y}{6}f(x, x), \tag{63}$$

$$\psi_{-1/2}(Y,x)=\left(\frac{-8Y}{3}+2\right)x+\frac{2Y}{3}\ln x+\frac{(-4Y+3)x-2Y}{6}f(x,x), \tag{64}$$

$$\psi_{\nu}(x)=\psi_{+1/2}(-1/2,x), \qquad \psi_{e}(x)=\psi_{-1/2}(-1/2,x), \tag{65}$$

$$\psi_{u}(x)=\psi_{+1/2}(1/6,x), \qquad \psi_{d}(x)=\psi_{-1/2}(1/6,x), \tag{66}$$

and the functions χ_+, θ_+, f are given in Appendix C.

B. Technicolor contribution

The technicolor contribution is due to the minimal walking technicolor model [6,7]. This is a walking technicolor theory whose strong coupling gauge theory dynamics are nonperturbative. However, the perturbative one-loop formulas are often used to estimate the leading contributions to S, T parameters, and we take this estimate as a guide also in this paper. Therefore, we obtain

$$S_{\rm TC}=\frac{N_D d[R]}{2\pi}[\psi_{+1/2}(Y,x_{\mathcal{T}})+\psi_{-1/2}(Y,x_{\mathcal{B}})], \tag{67}$$

$$T_{\rm TC}=\frac{N_D d[R]}{16\pi s_W^2 c_W^2}\theta_+(x_{\mathcal{T}},x_{\mathcal{B}}), \tag{68}$$

where $x_{\mathcal{T}}\equiv m_{\mathcal{T}}^2/M_Z^2$ and $x_{\mathcal{B}}\equiv m_{\mathcal{B}}^2/M_Z^2$, R denotes the representation of the technifermions under the technicolor gauge group, $d[R]$ is a dimension of the representation R, and N_D is the number of $SU(2)_L$ doublets. In the present model, we have $R=\square\square$, $d[\square\square]=3$, and $N_D=1$ with $Y=1/6$. When we take $m_{\mathcal{T}}=m_{\mathcal{B}}\gg M_Z$, Eqs. (67) and (68) are

$$S_{\rm TC}=\frac{1}{2\pi} \quad \text{and} \quad T_{\rm TC}=0. \tag{69}$$

Moreover, the S parameter indicates a decreasing tendency thanks to the walking dynamics [74–81]. The value of $S_{\rm TC}$ including an effect of the walking dynamics is estimated as $\sim S_{\rm TC}\times 0.7\simeq 0.1$ [75]. Because of the nonperturbative nature of these estimates, we will allow for a broader range of values, $S=0.1,\ldots,0.3$, in the study of the electroweak precision constraints for the present model in Sec. V.

C. Higgs contributions

The leading contributions to the S, T parameters from the dynamical Higgs sector are given by [43,45]

$$\begin{aligned}S_{\rm Higgs}=\frac{1}{\pi M_Z^2}[&\sin^2(\beta-\alpha)\bar{\mathcal{F}}'_2(M_Z^2,m_H^2,m_A^2)-\bar{\mathcal{F}}'_2(M_Z^2,m_{H^\pm}^2,m_{H^\pm}^2)+\cos^2(\beta-\alpha)\{\bar{\mathcal{F}}'_2(M_Z^2,m_h^2,m_A^2)\\&+\bar{\mathcal{F}}'_2(M_Z^2,m_Z^2,m_H^2)-\bar{\mathcal{F}}'_2(M_Z^2,m_Z^2,m_h^2)\}+\cos^2(\beta-\alpha)M_Z^2\{\mathcal{F}'_0(M_Z^2,m_Z^2,m_H^2)-\mathcal{F}'_0(M_Z^2,m_Z^2,m_h^2)\}],\end{aligned} \tag{70}$$

and

$$\begin{aligned}T_{\rm Higgs}=\frac{1}{16\pi s_W^2 c_W^2}[&\theta_+(x_{H^\pm},x_A)+\sin^2(\beta-\alpha)\{\theta_+(x_{H^\pm},x_H)-\theta_+(x_A,x_H)\}+\cos^2(\beta-\alpha)\{\theta_+(x_{H^\pm},x_h)\\&-\theta_+(x_A,x_h)\}+\cos^2(\beta-\alpha)\{\theta_+(x_W,x_H)-\theta_+(x_W,x_h)+4\bar{\mathcal{F}}'_0(M_W^2,m_H^2,m_h^2)\\&-\theta_+(x_Z,x_H)+\theta_+(x_Z,x_h)-4\bar{\mathcal{F}}'_0(M_Z^2,m_H^2,m_h^2)\}\Big],\end{aligned} \tag{71}$$

where

$$\bar{\mathcal{F}}'_2(q^2,m^2,M^2)=\frac{q^2}{2}\left[\frac{1}{6}\ln q^2-\mathcal{F}_2(q^2,m^2,M^2)+\mathcal{F}_2(0,m^2,M^2)\right], \tag{72}$$

$$\bar{\mathcal{F}}'_0(m^2,M_1^2,M_2^2)=\frac{m^2}{M_Z^2}[\mathcal{F}_0(0,m^2,M_1^2)-\mathcal{F}_0(0,m^2,M_2^2)], \tag{73}$$

and the functions $\mathcal{F}_{0,2}$, $\mathcal{F}'_0$, θ_+ are given in Appendix C.

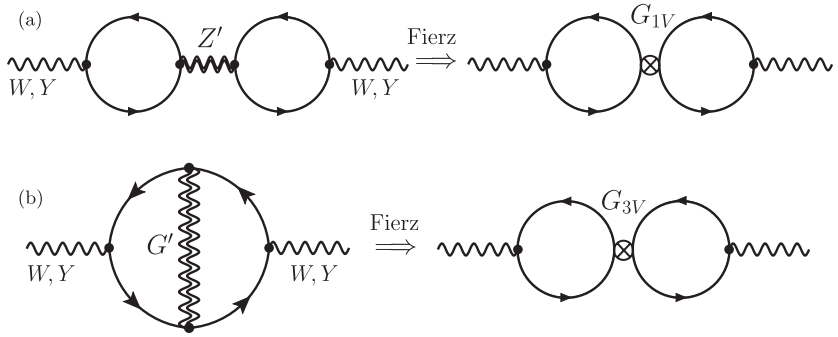

FIG. 3. (a) Z' and (b) G' contributions to the self-energy of the electroweak gauge bosons. The diagrams on the left show the leading Z', G' contribution which corresponds to the two-loop diagrams. The diagrams on the right show these diagrams after replacing the massive vector boson exchange by vector four-fermion interactions and Fierz rearranging [82]. As a result, the diagrams correspond to the product of two one-loop diagrams.

D. Coloron and Z' contributions

We should also take into account the contributions to the EWPT observables from the massive gauge bosons Z' and G'. As one can see from Eqs. (1) and (2), the leading contributions from Z' and G' to the self-energy of the electroweak gauge bosons are given by left diagrams in Fig. 3. Although these leading contributions are two-loop diagrams, they become a product of two one-loop diagrams after a Fierz rearrangement of the four-fermion interaction corresponding to the exchange of a heavy vector boson [82].

Among the four-fermion interactions given by Eqs. (4) and (5), the scalar four-fermion interactions to the vacuum polarizations of the electroweak gauge bosons appear as $\propto q^\mu q^\nu$, where q is the momentum of the electroweak gauge bosons. Hence, these do not contribute to the electroweak precision parameters. Because of this fact, we do not show $G_{1S,3S}$ in Fig. 3.

We will ignore the contribution from $SU(3)_2$ and $U(1)_{Y2}$ sectors because these are proportional to $\alpha_{\rm QCD}^2/\kappa_3$, $\alpha_Y^2/\kappa_1 \ll 1$, respectively, as shown in Eq. (1) and (2). Moreover, even though the third-generation leptons have $U(1)_{Y1}$ charge (see Table I) their masses are smaller than the masses of $u^{(3,4)}$, $d^{(3,4)}$ quarks, and hence we ignore also their contributions.

Let us now compute diagrams in Fig. 4 for a general case where $G_{1(2)} = g_{L1(2)}P_L + g_{R1(2)}P_R$. The coupling G_V ($\otimes$ in figure) is a vector four-fermion coupling which has a form as $[\cdots\gamma_\mu P_{L(R)}\cdots]\times[\cdots\gamma^\mu P_{L(R)}\cdots]$ as shown in Eq. (5), so we represent G_V as $G_V^{L\otimes L}$ and $G_V^{R\otimes R}$, respectively. For a case with $L\otimes L$, Fig. 4 is calculated as

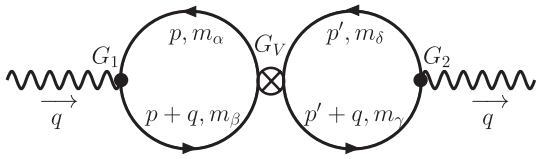

FIG. 4. For calculations.

$$\Pi^L(q^2) = -\frac{G_V^{L\otimes L}}{2}\left(\frac{3}{8\pi^2}\right)^2[g_{R1}m_\alpha m_\beta\bar{\mathcal{F}}_0(q^2,m_\alpha^2,m_\beta^2) - g_{L1}\bar{\mathcal{F}}_1(q^2,m_\alpha^2,m_\beta^2)][g_{R2}m_\delta m_\gamma\bar{\mathcal{F}}_0(q^2,m_\delta^2,m_\gamma^2) - g_{L2}\bar{\mathcal{F}}_1(q^2,m_\delta^2,m_\gamma^2)], \quad (74)$$

and for a case with $R\otimes R$, Fig. 4 is calculated as

$$\Pi^R(q^2) = -\frac{G_V^{R\otimes R}}{2}\left(\frac{3}{8\pi^2}\right)^2[g_{L1}m_\alpha m_\beta\bar{\mathcal{F}}_0(q^2,m_\alpha^2,m_\beta^2) - g_{R1}\bar{\mathcal{F}}_1(q^2,m_\alpha^2,m_\beta^2)][g_{L2}m_\delta m_\gamma\bar{\mathcal{F}}_0(q^2,m_\delta^2,m_\gamma^2) - g_{R2}\bar{\mathcal{F}}_1(q^2,m_\delta^2,m_\gamma^2)], \quad (75)$$

where

$$\bar{\mathcal{F}}_0(q^2,m^2,M^2) = \ln\frac{q^2}{\Lambda^2} + \mathcal{F}_0(q^2,m^2,M^2), \quad (76)$$

$$\bar{\mathcal{F}}_1(q^2,m^2,M^2) = q^2\left[\frac{2-3(x+y)}{6}\ln\frac{q^2}{\Lambda^2} + \mathcal{F}_1(q^2,m^2,M^2)\right], \quad (77)$$

and the functions $\mathcal{F}_{0,1}$ are given in Appendix C. In the present model, one can express each G_V in terms of quark mass eigenstates from Eqs. (5) and (16). The resulting vertex coefficients are given in Table II.

By substituting G_V in Table II and $g_{L,R}$ in Table III into Eqs. (74) and (75), and summing over all quark generations in loops, we obtain each $\Pi(q^2)$. For example, let us consider

$$\Pi_{3Y}(q^2) = \Pi_{3Y}^L(q^2) + \Pi_{3Y}^R(q^2), \qquad \Pi_{3Y}^{L,R}(q^2) = \Pi_{3Y}^{L,R}(q^2)|_u + \Pi_{3Y}^{L,R}(q^2)|_d. \quad (78)$$

For $\Pi_{3Y}^L(q^2)|_u$, one can read each $g_{L,R}$ from Table III as

TABLE II. The vector fourquark operators in terms of mass eigenstates for quarks which is derived from Eq. (5) with Eq. (16). The fermion with index $\alpha = 1, \ldots, 4$ has mass m_α in Fig. 4.

Four-fermion operators	$-iG_V^{L\otimes L}$ or $-iG_V^{R\otimes R}$
$[\bar{u}^{(\alpha)}\gamma^\mu P_L u^{(\beta)}][\bar{u}^{(\gamma)}\gamma_\mu P_L u^{(\delta)}]$	$-i[G_{3V} + \frac{1}{36}G_{1V}] \cdot (U^{L*}_{3\alpha}U^{L}_{3\beta}) \cdot (U^{L*}_{3\gamma}U^{L}_{3\delta})$
$[\bar{u}^{(\alpha)}\gamma^\mu P_R u^{(\beta)}][\bar{u}^{(\gamma)}\gamma_\mu P_R u^{(\delta)}]$	$-i[G_{3V} + \frac{4}{9}G_{1V}] \cdot (U^{R*}_{4\alpha}U^{R}_{4\beta}) \cdot (U^{R*}_{4\gamma}U^{R}_{4\delta})$
$[\bar{d}^{(\alpha)}\gamma^\mu P_L d^{(\beta)}][\bar{d}^{(\gamma)}\gamma_\mu P_L d^{(\delta)}]$	$-i[G_{3V} + \frac{1}{36}G_{1V}] \cdot (D^{L*}_{3\alpha}D^{L}_{3\beta}) \cdot (D^{L*}_{3\gamma}D^{L}_{3\delta})$
$[\bar{d}^{(\alpha)}\gamma^\mu P_R d^{(\beta)}][\bar{d}^{(\gamma)}\gamma_\mu P_R d^{(\delta)}]$	$-i[G_{3V} + \frac{1}{9}G_{1V}] \cdot (D^{R*}_{4\alpha}D^{R}_{4\beta}) \cdot (D^{R*}_{4\gamma}D^{R}_{4\delta})$
$[\bar{u}^{(\alpha)}\gamma^\mu P_L d^{(\beta)}][\bar{d}^{(\gamma)}\gamma_\mu P_L u^{(\delta)}]$	$-2i[G_{3V} + \frac{1}{36}G_{1V}] \cdot (U^{L*}_{3\alpha}D^{L}_{3\beta}) \cdot (D^{L*}_{3\gamma}U^{L}_{3\delta})$
$[\bar{u}^{(\alpha)}\gamma^\mu P_R d^{(\beta)}][\bar{d}^{(\gamma)}\gamma_\mu P_R u^{(\delta)}]$	$-2i[G_{3V} - \frac{2}{9}G_{1V}] \cdot (U^{R*}_{4\alpha}D^{R}_{4\beta}) \cdot (D^{R*}_{4\gamma}U^{R}_{4\delta})$

TABLE III. The quark-electroweak gauge boson couplings in mass eigenbasis of the quarks in the form of $\gamma^\mu[g_L P_L + g_R P_R]$ where $P_{L,R} = (1 \mp \gamma_5)/2$. α, $\beta = 1, 2, 3, 4$ and $\mathcal{V}$, $\mathcal{U}$, $\mathcal{D}$ are given in Eqs. (A3)–(A5).

Vertex	ig_L	ig_R
$g_2 W^+_\mu \bar{u}^{(\alpha)} d^{(\beta)}$	$i\frac{1}{\sqrt{2}}\mathcal{V}_{\alpha\beta}$	0
$g_2 W^3_\mu \bar{u}^{(\alpha)} u^{(\beta)}$	$i\frac{1}{2}\mathcal{U}^L_{\alpha\beta}$	0
$g_2 W^3_\mu \bar{d}^{(\alpha)} d^{(\beta)}$	$-i\frac{1}{2}\mathcal{D}^L_{\alpha\beta}$	0
$g_1 B_\mu \bar{u}^{(\alpha)} u^{(\beta)}$	$i[-\frac{1}{2}\mathcal{U}^L_{\alpha\beta} + \frac{2}{3}\delta_{\alpha\beta}]$	$i\frac{2}{3}\delta_{\alpha\beta}$
$g_1 B_\mu \bar{d}^{(\alpha)} d^{(\beta)}$	$i[\frac{1}{2}\mathcal{D}^L_{\alpha\beta} - \frac{1}{3}\delta_{\alpha\beta}]$	$-i\frac{1}{3}\delta_{\alpha\beta}$

$$
\begin{aligned}
g_{L1} &= (1/2)\mathcal{U}^L_{\beta\alpha}, \qquad g_{R1} = 0, \\
g_{L2} &= -(1/2)\mathcal{U}^L_{\delta\gamma} + (2/3)\delta_{\delta\gamma}, \qquad g_{R2} = (2/3)\delta_{\delta\gamma}, \\
G_V^{L\otimes L} &= [G_{3V} + (1/36)G_{1V}] \cdot (U^{L*}_{3\alpha}U^{L}_{3\beta}U^{L*}_{3\gamma}U^{L}_{3\delta}).
\end{aligned} \tag{79}
$$

Thus, we obtain

$$
\begin{aligned}
&\Pi^L_{3Y}(q^2)|_u \\
&= +\frac{1}{4}\left[G_{3V} + \frac{1}{36}G_{1V}\right]\left(\frac{3}{8\pi^2}\right)^2 \\
&\quad \times \sum_{\alpha,\beta,\gamma,\delta} [U^{L*}_{3\alpha}U^{L}_{3\beta}U^{L*}_{3\gamma}U^{L}_{3\delta}] \cdot \mathcal{U}^L_{\beta\alpha}\bar{\mathcal{F}}_1(q^2, m^2_\alpha, m^2_\beta) \\
&\quad \times \left\{\frac{2}{3}m^2_\gamma \bar{\mathcal{F}}_0(q^2, m^2_\gamma, m^2_\gamma) - \left(-\frac{1}{2}\mathcal{U}^L_{\delta\gamma} + \frac{2}{3}\delta_{\delta\gamma}\right)\right. \\
&\quad \left. \times \bar{\mathcal{F}}_1(q^2, m^2_\delta, m^2_\gamma)\right\}.
\end{aligned} \tag{80}
$$

For all other $\Pi(q^2)$'s, it is easy to obtain a similar representation as Eq. (80). By substituting each result for $\Pi(q^2)$ into Eqs. (54) and (55), we obtain $S_{G',Z'}$ and $T_{G',Z'}$; we do not present their formulas explicitly.

V. NUMERICAL RESULTS

In this section, we perform the numerical calculations for the present model by using the results derived in previous sections. In this paper, we fix $g^{(34)}_{U,D}$ in Eq. (10) as

$$
g^{(34)}_U = g^{(34)}_D + \tfrac{1}{9}\kappa_1 = 1.2 \quad \text{and} \quad \kappa_1 = 0.5, \tag{81}
$$

which satisfies the criticality condition $g^{(34)}_{U,D} > g_{\rm crit} = 1$ and the Landau pole constraint for $\Lambda_L/\Lambda = 10$ as one can see from Fig. 1. The value of $g^{(34)}_{U,D}$ is dictated to lie above but near the critical value by the requirement to reproduce correct masses for the third-generation quarks. The parameter κ_1 is constrained to lie in a narrow range $\kappa_1 < 0.6$ by the Landau pole constraint, and the results are not heavily affected by its value.

Moreover, we assume that the quark mixing matrices Eq. (16) reflect the seesaw mechanism for the third and fourth generations. This implies that the third- and fourth-generation mixing will dominate these matrices. Thus, at the leading order, these matrices are [43] $(0 < \theta^{u,d}_{L,R} < \pi/2)$,

$$
\begin{aligned}
U^L_{\alpha\beta} &\simeq \begin{pmatrix} 1 & 0 & 0 & 0 \\ 0 & 1 & 0 & 0 \\ 0 & 0 & \cos\theta^u_L & \sin\theta^u_L \\ 0 & 0 & -\sin\theta^u_L & \cos\theta^u_L \end{pmatrix}, \\
U^R_{\alpha\beta} &\simeq \begin{pmatrix} 1 & 0 & 0 & 0 \\ 0 & 1 & 0 & 0 \\ 0 & 0 & -\cos\theta^u_R & \sin\theta^u_R \\ 0 & 0 & \sin\theta^u_R & \cos\theta^u_R \end{pmatrix},
\end{aligned} \tag{82}
$$

and similarly for $D^L_{\alpha\beta}$ and $D^R_{\alpha\beta}$ by replacing $u \to d$ in the above definitions. With these matrices, we diagonalize the mass terms in which the dynamical mass term $\Sigma_U \bar{U}^3_L U^{(4)}_R + \Sigma_D \bar{D}^3_L D^{(4)}_R$, together with its Hermitian conjugate, is combined with Eq. (11), and we identify each eigenvalues as the third-generation quark masses m_t, m_b and the fourth-generations quarks masses $m_{t'}(>m_t)$, and $m_{b'}(>m_b)$. The eigenvalues $m_{t'}$ and $m_{b'}$ are related to given m_t and m_b as

$$
m_{t'} = m_t \cdot [\cot\theta^u_L \cot\theta^u_R], \qquad m_{b'} = m_b \cdot [\cot\theta^d_L \cot\theta^d_R], \tag{83}
$$

where $m_t = 172.9$ GeV and $m_b = 4.2$ GeV. We note that the above mixing matrices are only a leading approximation, and more refined structures may be inferred from phenomenology. For example, in order to explain the Tevatron anomaly in the top-quark forward-backward asymmetry [83] by the model of this type, one may

need a mixing between the light quarks and the heavy third-generation quarks [84]. However, since these effects are subleading and we do not aim to explain the Tevatron anomaly quantitatively, we will use Eq. (82) as the quark mixing matrices in our analysis here.

Under these assumptions, and for given $\Lambda = M_{G',Z'}$ and topcolor instanton parameter ξ in Sec. III B, we now proceed to calculate numerically

(i) masses of the fourth-generation quarks t', b' by solving the gap equations Eqs. (17) and (18),
(ii) dynamical Higgs masses derived in Sec. III B,
(iii) the Peskin-Takeuchi S, T parameters as given in Sec. IV.

A. Dynamical results for mass spectrums of fourth-generation quarks and Higgs

When we substitute $m_{t',b'}$ given by Eq. (83) into the gap equations (17) and (18), the resulting equations depend only on $\theta^{u,d}_{L,R}$ and $m_{t,b}$; the couplings $g^{(34)}_{U,D}$ take the values given in Eq. (81). Since the dynamical symmetry breaking derived from $g^{(34)}_{U,D} > g_{\rm crit}$ gives only a part of the electroweak gauge boson masses, we should solve the resultant gap equations under conditions in which the decay constants Eqs. (52) and (53) together with $v_{\rm TC}$ satisfy $v_1^2 + v_2^2 + v_{\rm TC}^2 = v_{\rm EW}^2$, where $v_{\rm EW} = 246$ (GeV). This condition is more conveniently written as

$$v_1^2 + v_2^2 = v_{\rm EW}^2 \cdot \cos^2\phi, \tag{84}$$

where $\tan^2\phi = v_{\rm TC}^2/(v_1^2 + v_2^2)$.

In this paper, we assume the walking technicolor sector has characteristics of a low-scale technicolor model [35–37], meaning that we set $\tan\phi \leq 1$. In the limit $\tan\phi = 0$, we obtain the original top-quark seesaw model. Moreover, $T_{G',Z'}$ in the topcolor model becomes large and *positive* at $\Lambda \simeq \mathcal{O}$ (TeV) [82], on the other hand, T_{4q} in the top-seesaw model becomes large and *negative* at $\Lambda \simeq \mathcal{O}$ (TeV) [43], so we can expect a cancellation between $T_{G',Z'}$ and T_{4q} at $\Lambda \simeq \mathcal{O}$ (TeV) if we take $\tan\beta = v_2/v_1 \leq 1$. Specifically, we will consider two special cases $\tan\phi = 0$, 1 with $\tan\beta = 1$ in the following.

In Fig. 5, we show the numerical results for $m_{t',b'}$ and $m_{t'} - m_{b'}$ and in Fig. 6 for m_{A^0}, $m_{H^\pm}$, m_{h^0}, and m_{H^0} when 2 TeV $\leq \Lambda \leq$ 100 TeV, $\tan\beta = 1$, and $\tan\phi = 0$, 1. We reproduce the results of [43] at the limit $\kappa_1 = 0$ and $\tan\phi = 0$ in our model. As $\tan\phi \to 0$, mass splitting $m_{t'} - m_{b'}$ becomes small at $\Lambda \simeq \mathcal{O}$ (TeV) and, due to the restoration of the custodial symmetry, $m_{H^\pm} \simeq m_{h^0} \simeq m_{H^0}$ at $\Lambda \simeq \mathcal{O}$ (TeV). We find that, as $\tan\phi \to 1$, κ_1 tends to influence the mass splitting even if the cutoff scale is several TeV. From Fig. 6, we can see easily that dynamical Higgs mass in the present model can be smaller than in the top-quark seesaw model. In the present model, the light CP-even neutral Higgs mass M_{h^0} is 400–500 GeV which is smaller than $M_{h^0} = 700$–900 GeV obtained in the top-quark seesaw model. This is so due to the existence of the technicolor sector which allows $v_1^2 + v_2^2$ to be small in the limit $\tan\phi \to 1$.

B. The Peskin-Takeuchi S, T parameters

To consider the electroweak precision tests (EWPT), we need the constraints for Peskin-Takeuchi S, T, U parameters [5] from the electroweak precision data. In this paper, we use values in [85] as

$$S = 0.03 \pm 0.09, \qquad T = 0.07 \pm 0.08, \tag{85}$$

and a correlation $\rho_{ST} = 0.87$ for a reference Higgs mass $m_h^{\rm ref} = 117$ GeV. Note that these values for S, T parameters differ with respect to [86]. This is because [85] fix

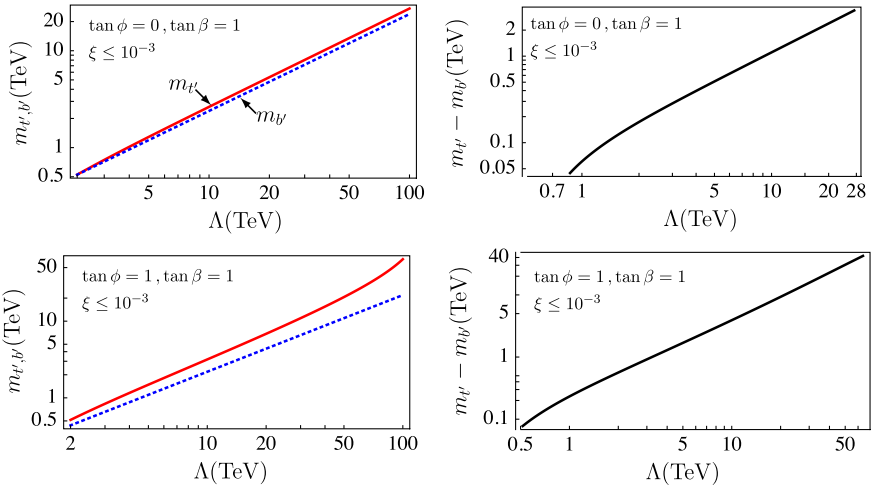

FIG. 5 (color online). The dynamical results for fourth-generation quarks. The left and right panels show $m_{t'}$(TeV) (red/solid lines) and $m_{b'}$(TeV) (blue/dotted lines) and $m_{t'} - m_{b'}$(TeV), respectively. From top to bottom, $(\tan\phi, \tan\beta) = (0, 1), (1, 1)$ with $\xi \leq 10^{-3}$. The topmost figures correspond to the top-quark seesaw model in [43] with $g = 1.2$ and $\kappa_1 = 0$.

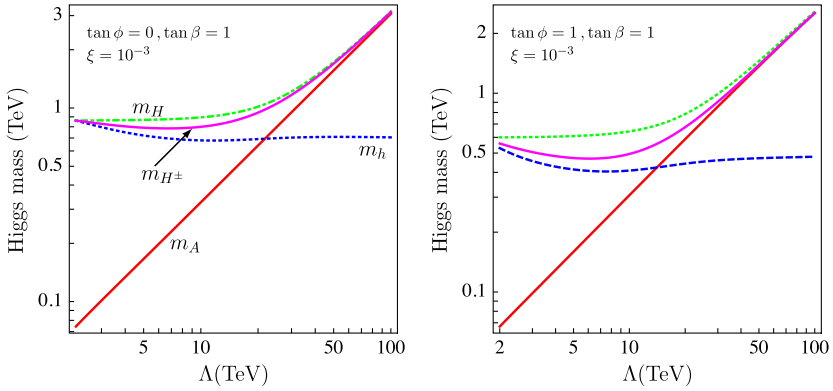

FIG. 6 (color online). The dynamical results for *Higgs* mass for 2 TeV $\leq \Lambda \leq$ 100 TeV. In all figures, m_{A^0}, $m_{H^\pm}$, m_{h^0}, m_{H^0} are represented as solid/red lines, solid/magenta lines, dotted/blue lines, and dash-dotted/green lines, respectively. These panels are $(\tan\phi, \tan\beta) = (0, 1)$ (left) and (1, 1) (right). The left panel corresponds to the top-quark seesaw model in [43] with $g = 1.2$, $\kappa_1 = 0$, and $\xi = 10^{-3}$.

$U = 0$, i.e. for a two-parameter fit, while the estimation in [86] is for a three-parameter fit.

In our model, there are several sources contributing to the precision parameters, and to understand various effects we consider different contributions separately before presenting the full analysis. In Fig. 7, we show $S_{4q} + S_{\rm Higgs} + S_{G',Z'}$ for 2 TeV $\leq \Lambda \leq$ 50 TeV, and also the corresponding contribution to the T parameter. In the evaluation of these quantities, we use the dynamical results obtained in previous sections. In addition, for comparison, we also show $S_{4q} + S_{\rm Higgs}$ and $S_{G',Z'}$ (and the corresponding contributions to the T parameters) in Fig. 7. From these figures, we see, as we had expected, that the massive gauge boson contribution cancels with a large contribution from the dynamical seesaw sectors, i.e. vectorlike quarks and the resultant Higgs contributions for the T parameter. As to the S parameter, the massive gauge bosons contributions are smaller than the contributions from the dynamical seesaw sectors. Unfortunately, a total value of the S parameter coming from the topcolor sectors is too large for a low Λ; a result already obtained in [43]. But, in the present model, there are the fourth-family leptons which can make a negative contribution to the S parameter for a suitable mass difference between $N^{(4)}$ and $E^{(4)}$. In Fig. 8, we show total S, T parameters in the present model. In this figure, the solid (dashed) ellipsis, obtained from Eq. (85) shows

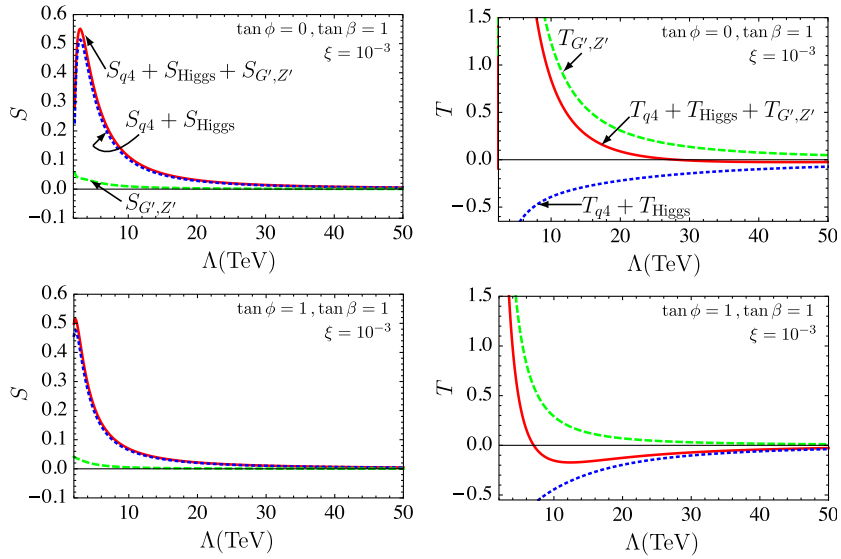

FIG. 7 (color online). The Peskin-Takeuchi S parameter (left panels) and T parameter (right panels) coming from the fourth-generation quarks in Sec. IV A, the dynamical Higgs in Sec. IV C and G', Z' in Sec. 4 D for 2 TeV $\leq \Lambda \leq$ 50 TeV. In all figures, the dashed/green curves, the dotted/blue curves, and the solid/red curves correspond to $S(\text{or}\,T)_{G',Z'}$, $S(\text{or}\,T)_{4q} + S(\text{or}\,T)_{\rm Higgs}$, and $S(\text{or}\,T)_{4q} + S(\text{or}\,T)_{\rm Higgs} + S(\text{or}\,T)_{G',Z'}$, respectively. Top and bottom panels correspond to $(\tan\phi, \tan\beta) = (0, 1), (1, 1)$. The top figures correspond to the top-quark seesaw model in [43] with $g = 1.2$ and $\kappa_1 = 0$.

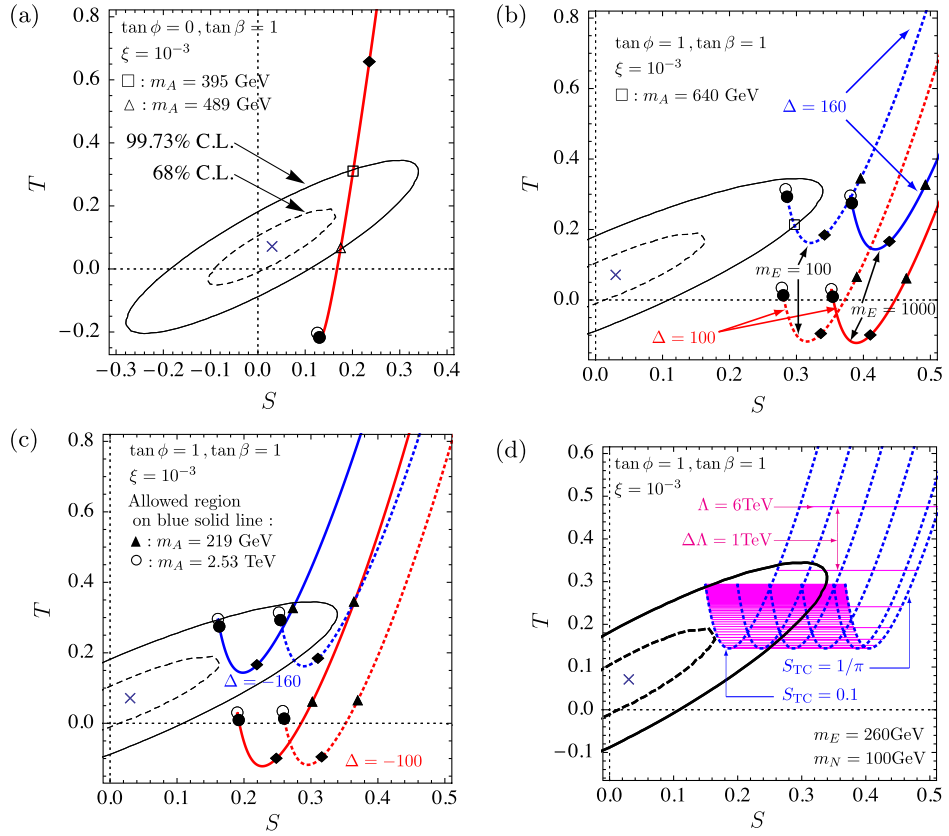

FIG. 8 (color online). The Peskin-Takeuchi S, T parameters in the present model with experimentally allowed contour at 99.73% (68%) C.L., corresponding to the solid (dashed) ellipsis. Panel (a) corresponds to $(\tan\phi, \tan\beta) = (0, 1)$ and (b, c) correspond to $(\tan\phi, \tan\beta) = (1, 1)$. In panel (b), the upper (lower) set of two curves corresponds to $\Delta \equiv m_N - m_E = 160(100)$ GeV with $m_E = 100$ GeV (solid curve) and 1000 GeV (dotted curve). In panel (c), the upper (lower) curves correspond to $\Delta = -160(-100)$ GeV with $m_N = 100$ GeV (solid curve) and 1000 GeV (dotted curve). On each curve, the symbols ▲, ◆, •, and ○ correspond to $\Lambda = 7$ TeV, 10 TeV, 50 TeV, and 100 TeV, respectively. In panel (a), □ and △ correspond to $(\Lambda(\text{TeV}), m_A(\text{GeV})) = (12, 395)$ and $(15, 489)$. In panel (b), □ on the dotted line with $\Delta = 170$ corresponds to $(\Lambda(\text{TeV}), m_A(\text{GeV})) = (15.9, 474)$, and in panel (c), ▲ and ○ on the solid line with $\Delta = -160$ correspond to $(\Lambda(\text{TeV}), m_A(\text{GeV})) = (7, 219)$ and $(\Lambda(\text{TeV}), m_A(\text{TeV})) = (100, 2.5)$, respectively. In panel (d), for a case with $(m_N(\text{GeV}), m_E(\text{GeV})) = (100, 260)$, the dotted lines correspond to $S_{\text{TC}} = 0.1, 0.15, 0.2, 0.25, 0.3, 1/\pi$ from right to left. The horizontal (magenta, solid) lines in (d) show various Λ from 6 TeV to 100 TeV at intervals of $\Delta\Lambda(\text{TeV}) = 1$.

the experimentally allowed contour at 99.73% (68%) C.L. Panel (a) corresponds to $(\tan\phi, \tan\beta) = (0, 1)$, i.e. the top-quark seesaw model in [43] with $g = 1.2$ and $\kappa_1 = 0$. In panels (b) and (c), we have set $(\tan\phi, \tan\beta) = (1, 1)$, and the curves show how the model results are affected by the masses of fourth-generation leptons. In panel (b), the upper (lower) set of two curves corresponds to $\Delta \equiv m_N - m_E = 160(100)$ GeV with $m_E = 100$ GeV (solid curve) and 1000 GeV (dotted curve), while in panel (c) the upper (lower) curves correspond to $\Delta = -160(-100)$ GeV with $m_N = 100$ GeV (solid curve) and 1000 GeV (dotted curve). On each curve, the symbols ▲, ◆, •, and ○ correspond, respectively, to $\Lambda = 7$ TeV, 10 TeV, 50 TeV, and 100 TeV. In panel (a), the symbols □ and △ correspond to $(\Lambda(\text{TeV}), m_A(\text{GeV})) = (12, 395)$ and $(15, 489)$. In panel (b), the symbol □ on the dotted line corresponds to $(\Lambda(\text{TeV}), m_A(\text{GeV})) = (21.9, 640)$. In panel (c), the symbols ▲ and ○ on the solid line correspond to $(\Lambda(\text{TeV}), m_A(\text{GeV})) = (7, 219)$ and $(\Lambda(\text{TeV}), m_A(\text{TeV})) = (100, 2.5)$, respectively. In (a), (b), (c), the value of S_{TC} is fixed with 0.1. In order to see the dependence with S_{TC}, in panel (d), we show various case with varying S_{TC} from 0.1 to $1/\pi$ with $(m_N(\text{GeV}), m_E(\text{GeV})) = (260, 100)$. The left-most dotted curve in (d) corresponds to the upper solid line in panel (c).

We can see from these figures that if we take $\tan\phi = 1$ and $\Delta = m_N - m_E = -160$ GeV with $m_N = 100$ GeV–1 TeV we can take the cutoff as low as $\Lambda = 7$ TeV and the CP-odd Higgs A^0 mass is around 200 GeV with $m_{t'} \simeq 2.1$ TeV and $m_{b'} \simeq 1.5$ TeV. Such a light CP-odd Higgs is not allowed in the top-quark seesaw model with $\tan\beta = 1$. In fact, we can see from Fig. 8(a), together with results from Fig. 6(a), that the allowed mass region is given by 395 GeV $\lesssim m_{A^0} \lesssim$ 490 GeV in a case of the top-quark seesaw model with $\tan\beta = 1$ and $\xi = 10^{-3}$.

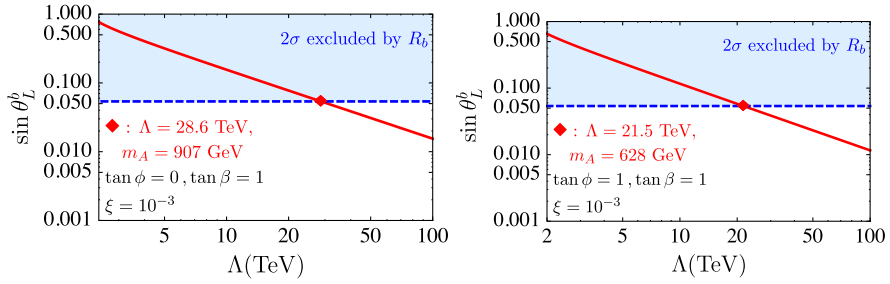

FIG. 9 (color online). R_b constraint on $(\Lambda, \sin\theta_L^b)$ plane for the present model with parameters $(\tan\phi, \tan\beta) = (0, 1)$ (left) and $(1, 1)$ (right) and $\xi = 10^{-3}$. The red/solid line corresponds to $\sin\theta_L^b(\Lambda)$, which is obtained as dynamical solution, the blue dashed line corresponds to 2σ R_b constraint, and the shaded region above the blue dashed line is 2σ excluded region. The diamond in both figures shows the 2σ lower bound for Λ, i.e. the lower bound is $(\Lambda(\text{TeV}), m_A(\text{GeV})) = (28.6, 907)$ (left) and $(21.5, 628)$ (right). The left panel corresponds to the top-quark seesaw model in [43] with $g = 1.2$ and $\kappa_1 = 0$.

We note that relative to the accuracy of the precision data, the largest uncertainty is in the S parameter of the technicolor sector. However, as we have shown, our model features several other sources to S and T, which are perturbatively under control. Hence, the analysis presented in this section will be useful in indicating how the model parameters can be used to assess the viability of the model if the contributions from the technicolor sector can be determined more precisely by using, say, lattice simulations.

C. R_b constraint

In the present model, we should take into consideration a constraint for $Zb\bar{b}$ vertex since, in general, this constraint is stronger than the constraint on the S, T plane in the top-quark seesaw model [43]. In this paper, it is enough to consider only the quark sector although the dynamical Higgs sector contributes to the $Zb\bar{b}$ vertex at the one-loop level. This is so since the latter contribution is large when $H^\pm$ is light as $m_{H^\pm} \simeq 200$ GeV [87], which is not the case in the scenarios we consider; see e.g. Fig. 6. Therefore, it is enough to consider only the tree-level contribution to the $Zb\bar{b}$ vertex in the present paper.

The experimental value of R_b [88] is

$$R_b^{\text{exp}} \equiv \frac{\Gamma(Z \to \bar{b}b)}{\Gamma(Z \to \text{had})} = 0.216\,29 \pm 0.000\,66. \tag{86}$$

It is convenient to divide $R_b = R_b^{\text{SM}} + \Delta R_b$, where R_b^{SM} is presented as [88]

$$R_b^{\text{SM}} = 0.215\,78^{+0.000\,05}_{-0.000\,08}. \tag{87}$$

The quantity ΔR_b then encapsulates the contribution from the new physics (NP), and is represented as

$$\Delta R_b = 2R_b^{\text{SM}}(1 - R_b^{\text{SM}})\,\text{Re}\left[\frac{g_L^b[\delta g_L^b]_{\text{NP}} + g_R^b[\delta g_R^b]_{\text{NP}}}{(g_L^b)^2 + (g_R^b)^2}\right]. \tag{88}$$

The experimental data constrains its value as

$$\Delta R_b = 0.000\,51 \pm 0.000\,66. \tag{89}$$

Equation (88) is derived straightforwardly from [89] and $g_{L,R}^b$ is the SM tree-level value given by

$$g_L^b = -\tfrac{1}{2} + \tfrac{1}{3}\sin^2\theta_W, \qquad g_R^b = \tfrac{1}{3}\sin^2\theta_W. \tag{90}$$

In the present model, a contribution to the $Zb\bar{b}$ vertex is given by [43]

$$\delta g_L^b = \frac{e}{2s_W c_W}\sin^2\theta_L^b, \qquad \delta g_R^b = 0, \tag{91}$$

where $e = \sqrt{4\pi\alpha}$ with $\alpha \simeq 1/128$. We show the resulting constraint in the $(\Lambda, \sin\theta_L^b)$ plane for the present model in Fig. 9. The solid line shows the dynamical solution $\sin\theta_L^b(\Lambda)$ obtained from the model, while the dashed horizontal line corresponds to the 2σ constraint on R_b; the shaded region above this line is excluded. We can read off from Fig. 9 that the lower bound is $(\Lambda, m_A) = (28.6\ \text{TeV}, 907\ \text{GeV})$ for $(\tan\beta, \tan\phi) = (1, 0)$ and $(\Lambda, m_A) = (21.5\ \text{TeV}, 628\ \text{GeV})$ for $(\tan\beta, \tan\phi) = (1, 1)$. Comparing these results with the EWPT parameters results as shown in Fig. 8 illustrates the fact that the R_b constraint is stronger than the EWPT constraints in this type of model [43]. We find that in the case with $(\tan\beta, \tan\phi) = (1, 0)$ there is no overlap between the EWPT parameters constraint and the R_b constraint. However, in the case with $(\tan\beta, \tan\phi) = (1, 1)$ there is allowed overlap: e.g. 628 GeV $\le m_A \le$ 2.53 TeV corresponding to 21.5 TeV $\le \Lambda \le$ 100 TeV thanks to the existence of the fourth-family leptons with $(m_N, m_E) = (100\ \text{GeV}, 260\ \text{GeV})$.

Note that these results may be sensitive to the contribution from the vector mesons in the MWT sector as shown in [90,91]. However, these results were derived for effective theory defined on the coset space $SU(2)_L \times SU(2)_R/SU(2)_V$ while G/H in the MWT is $SU(4)/SO(4)$.

D. LHC phenomenology

In this section, we consider the model in light of present and future LHC data. The mass of the color-octet vector

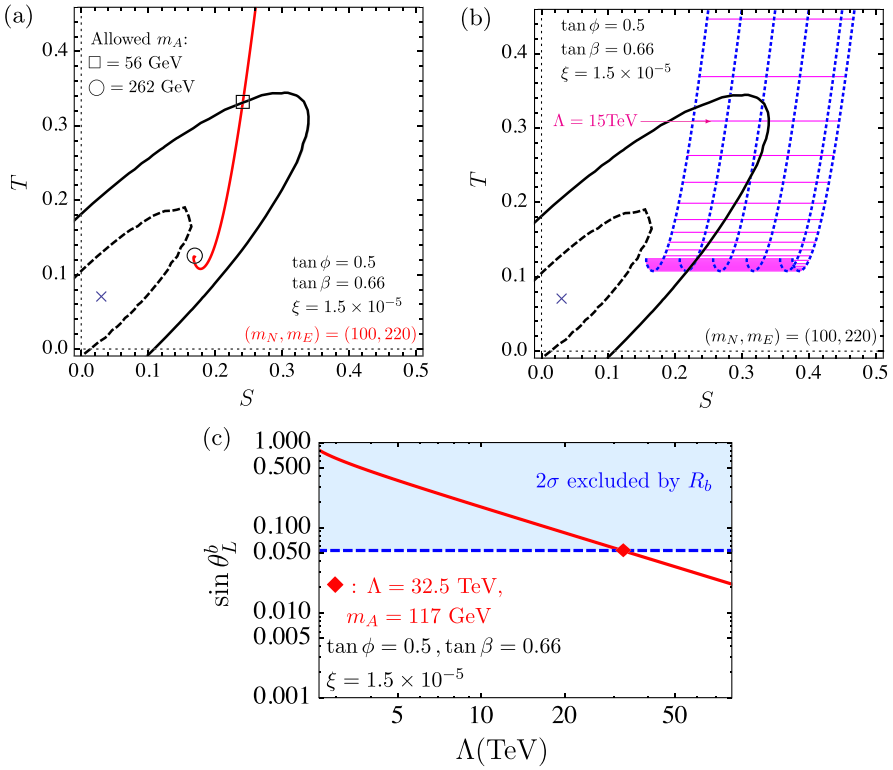

FIG. 10 (color online). (a), (b) The Peskin-Takeuchi S, T parameters (a) for $S_{\rm TC} = 0.1$ and (b) for varying $S_{\rm TC}$ and (c) R_b constraints (right panels) for the present model with $(\tan\phi, \tan\beta) = (0.5, 0.66)$, $\xi = 1.5 \times 10^{-5}$, and $(m_N, m_E) = (100\ \text{GeV}, 220\ \text{GeV})$. The allowed region for m_A is 117 GeV $\leq m_A \leq$ 262 GeV for $S_{\rm TC} = 0.1$.

boson is given by $M_{G'} = \Lambda$, and at 95% C.L. $M_{G'} > 3.32$ TeV [92]. Hence, the 4th-family quarks are constrained by $m_{t'} > 900$ GeV and $m_{b'} > 700$ GeV for $\tan\beta = \tan\phi = 1$, as we can read off from Fig. 5. These constraints for the 4th-family quark masses are consistent with $m_{t'} > 422$ GeV at 95 %C.L. [93], $m_{t'} > 450$ GeV at 95% C.L. [94] and $m_{b'} > 361$ GeV at 95% C.L. [95]. On the other hand, the lightest PNGBs of the model may be discovered in the LHC data when considering the SM Higgs boson production via the gluon fusion and decay into two photons [96,97]. We consider next this possibility.

In the model spectrum, there are two objects which can be discovered in the same decay mode as the SM Higgs boson: the lightest CP-odd neutral PNGB A^0 or the lightest CP-even neutral boson h^0, which are composed of 3rd- and 4th-family quarks. To study this possibility, we set parameters as $(\tan\phi, \tan\beta) = (0.5, 0.66)$ with $\xi = 1.5 \times 10^{-5}$. We take this choice of parameters simply as an example to illustrate the viability of the model in light of recent LHC data, and leave a more thorough scan of the parameter space for future work. With this choice of parameters, we can solve the gap equations (17) and (18) only for 2.6 TeV $\leq \Lambda \leq$ 80 TeV. We show the S, T parameters constraint and R_b constraint for these cases in Fig. 10. The 99.73% C.L. allowed region by the Peskin-Takeuchi S, T parameters (left panels in Fig. 10) is 14.6 TeV $\leq \Lambda \leq$ 80 TeV which corresponds to 56 GeV $\leq m_A \leq$ 262 GeV for $(m_N, m_E) = (100\ \text{GeV}, 220\ \text{GeV})$. The allowed region by the R_b constraints is 32.5 TeV $\leq \Lambda$ which corresponds to 117 GeV $\leq m_A$. Thus, in the present model with these parameters, the allowed region for m_A is 117 GeV $\leq m_A \leq$ 262 GeV. In this range, mass of the lightest CP-even Higgs: h^0 is 336 GeV $\leq m_h \leq$ 390 GeV.

Next, we will consider how this spectrum of light A^0 and h^0 is constrained by the LHC results for the SM Higgs. On one hand, the SM Higgs boson whose mass is within this range quoted above decays mainly to WW/ZZ. Hence, we should compare the h^0 with the results for the SM Higgs search in $h \to WW \to l\nu jj$ at the ATLAS [98], $h \to WW \to l\nu l\nu$ channel at the CMS [99], and $h \to ZZ \to 4l$ channel at the ATLAS [100] and the CMS [101]. On the other hand, similarly to the ordinary two-Higgs-doublet model, the A^0 here does not have any coupling with WW/ZZ at the tree level, so it is natural to concentrate only on the $A^0 \to \gamma\gamma$ channel. Thus, with the above parameter choices, we consider the ratios defined as

$$R_{gg\to\varphi\to X} \equiv \kappa_{gg}^{\varphi} \times \frac{\mathrm{Br}(\varphi \to X)}{\mathrm{Br}(h_{\rm SM} \to X)}, \tag{92}$$

where $\varphi = h^0, A^0$, $\mathrm{Br}(\varphi \to X) \equiv \Gamma(\varphi \to X)/\Gamma_{\rm tot}$,

$$\kappa_{gg}^{\varphi} = \frac{\sigma(gg \to \varphi)}{\sigma(gg \to h_{\rm SM})} = \frac{\Gamma(\varphi \to gg)}{\Gamma(h_{\rm SM} \to gg)}. \tag{93}$$

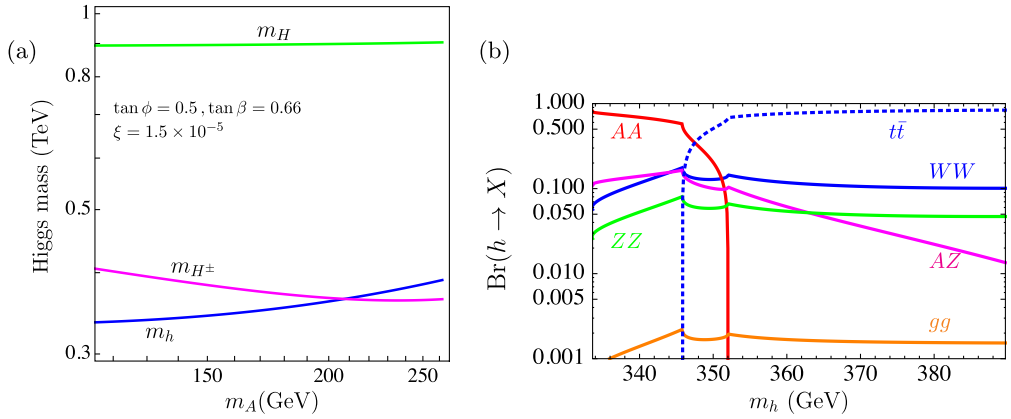

FIG. 11 (color online). (a) The dynamical results for Higgs masses and (b) the branching ratio Br($h \to X$) in the present model with $(\tan\phi, \tan\beta) = (0.5, 0.66)$ with $\xi = 1.5 \times 10^{-5}$ in the range of the allowed region by Fig. 10. (a): The dynamical results and the horizontal axis is the m_A(GeV) with 117 GeV $\leq m_A \leq$ 262 GeV. (b): The branching ratio of h^0 with 336 GeV $\leq m_h \leq$ 390 GeV.

In the SM, $\Gamma(h_{\rm SM} \to gg)$ is given by [102]

$$\Gamma(h_{\rm SM} \to gg) = \frac{\alpha_s^2 m_h^3}{32\pi^3 v_{\rm EW}^2} \left| \sum_{i=t,b} \tau_i A^{(h)}(\tau_i) \right|^2, \qquad (94)$$

and we will use the values of Br($h_{\rm SM} \to X$) given in [103]. The total decay widths, $\Gamma_{\rm tot}(\varphi)$ for $m_\varphi < 2m_{t',b'}$(≃ few TeV), are given by

$$\begin{aligned}\Gamma_{\rm tot}(h^0) = {} & \Gamma(h^0 \to gg) + \Gamma(h^0 \to \gamma\gamma) + \Gamma(h^0 \to t\bar{t}) \\ & + \Gamma(h^0 \to b\bar{b}) + \Gamma(h^0 \to WW) + \Gamma(h^0 \to ZZ) \\ & + \Gamma(h^0 \to A^0A^0) + \Gamma(h^0 \to A^0Z), \qquad (95)\end{aligned}$$

$$\begin{aligned}\Gamma_{\rm tot}(A^0) = {} & \Gamma(A^0 \to gg) + \Gamma(A^0 \to \gamma\gamma) \\ & + \Gamma(A^0 \to t\bar{t}) + \Gamma(A^0 \to b\bar{b}). \qquad (96)\end{aligned}$$

The decay widths appearing in above equations are explicitly given in Appendix D.

In Fig. 11, with model parameters $(\tan\phi, \tan\beta) = (0.5, 0.66)$ with $\xi = 1.5 \times 10^{-5}$ and within the region allowed by Fig. 10, we show in panel (a) the results for the dynamical Higgs masses with respect to m_A(GeV) in the range 117 GeV $\leq m_A \leq$ 262 GeV, and in panel (b) the branching ratio Br($h \to X$) with respect to m_h(GeV) in the range 336 GeV $\leq m_h \leq$ 390 GeV. As one can see from Fig. 11(a), in the present case, h^0 can decay mainly into A^0A^0 but h^0 cannot decay into $H^+H^-/H^\pm W^\mp$. Moreover, as one can read off from Fig. 11(b), if the $h^0 \to A^0A^0$ channel is kinematically allowed, this decay channel is the dominant decay mode, i.e. $h^0 \to WW/ZZ$ channel is suppressed. This is different from the SM Higgs case where $h^0_{\rm SM} \to WW/ZZ$ channel is dominant in this mass range of h^0.

Based on above results, we show $R_{gg\to h\to WW/ZZ}$ with the allowed range of m_h in Fig. 12. In the present case, gluon fusion process is enhanced compared with the SM Higgs case, $\kappa^h_{gg} \simeq 4$. However, the Br($h^0 \to WW/ZZ$) is

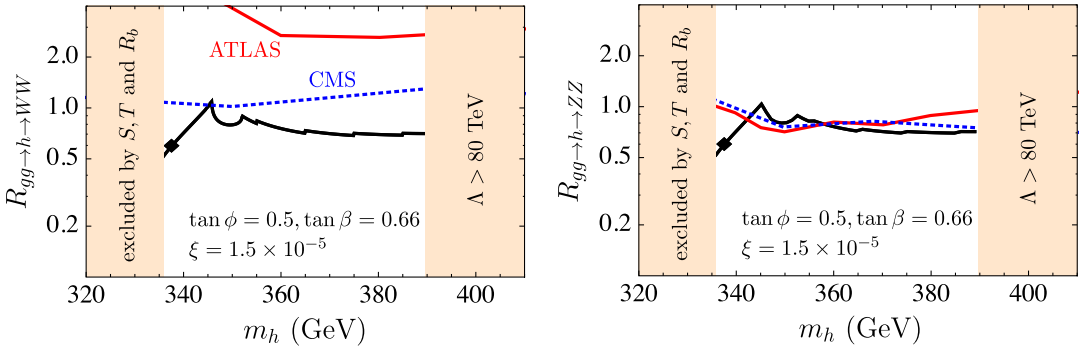

FIG. 12 (color online). $R_{gg\to h\to WW}$ (left) and $R_{gg\to h\to ZZ}$ (right) in the present model with $(\tan\phi, \tan\beta) = (0.5, 0.66)$ and $\xi = 1.5 \times 10^{-5}$. The lower/black solid lines in each figure correspond to $R_{gg\to h\to WW/ZZ}$ in the present model, the upper/red solid lines correspond to 95% C.L. observed upper limit on $R_{gg\to h\to WW/ZZ}$ for the SM Higgs boson decay into WW/ZZ at the ATLAS [98,100], and the blue/dotted lines correspond to 95% C.L. observed upper limit on $R_{gg\to h\to WW/ZZ}$ for the SM Higgs boson decay into WW/ZZ at the CMS [99,101]. In both figures, \diamondsuit implies the point at $\Lambda = 35.3$ TeV corresponding to $(m_A, m_h) =$ (126 GeV, 338 GeV). $\Lambda > 80$ TeV implies that the gap equations (17) and (18) do not have any solutions.

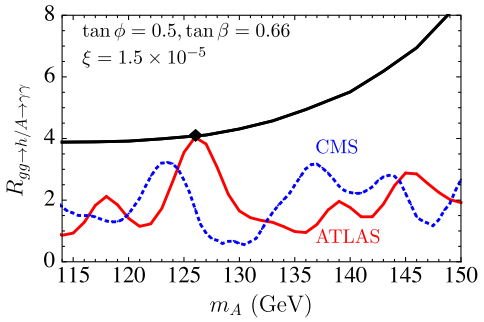

FIG. 13 (color online). $R_{gg\to h/A\to\gamma\gamma}$ in the present model with $(\tan\phi, \tan\beta) = (0.5, 0.66)$ with $\xi = 1.5 \times 10^{-5}$. The upper/black solid line corresponds to $R_{gg\to A\to\gamma\gamma}$ in the present model, the lower/red solid line corresponds to 95% C.L. observed upper limit on $R_{gg\to h\to\gamma\gamma}$ in the SM Higgs boson decay into two photons at the ATLAS [96], and the dotted/blue line corresponds to 95% C.L. observed upper limit on $R_{gg\to h\to\gamma\gamma}$ at the CMS [97]. \diamondsuit implies the point at $\Lambda = 35.3$ TeV corresponding to $(m_A, m_h) = (126\ \text{GeV}, 338\ \text{GeV})$.

suppressed as $\text{Br}(h^0 \to WW/ZZ)/\text{Br}(h^0_{\text{SM}} \to WW/ZZ) \simeq 0.18$ for $336\ \text{GeV} \leq m_h \leq 390\ \text{GeV}$. Thus, the present model gives $R_{gg\to h\to WW/ZZ} \simeq 0.8$ which should be compared with the LHC results [98–101]. Figure 12 shows that light CP-even Higgs h^0 with $342\ \text{GeV} \leq m_h \leq 357\ \text{GeV}$ is excluded at 95% C.L. which corresponds to $41.5, \text{TeV} \leq \Lambda \leq 55.5\ \text{TeV}$, and $146\ \text{GeV} \leq m_A \leq 190\ \text{GeV}$ in the present case.

Thus, we find the CP-odd Higgs A^0 in this model with $117\ \text{GeV} \leq m_A \leq 146\ \text{GeV}$ is allowed in light of the present data. Based on this result, we consider $R_{gg\to A\to\gamma\gamma}$ in the present model with $(\tan\phi, \tan\beta) = (0.5, 0.66)$ and $\xi = 1.5 \times 10^{-5}$. In Fig. 13, we show $R_{gg\to A\to\gamma\gamma}$ in the present case together with the 95% C.L. observed upper limit on $R_{gg\to h_{\text{SM}}\to\gamma\gamma}$ at the ATLAS [96] and the CMS [97]. This means that the excess around 126 GeV of only $\gamma\gamma$-channel in the ATLAS and CMS data implies a signal of neutral top-pion i.e. CP-odd Higgs A^0 in the present model since the neutral top-pion is EW-gaugephobic. In addition, in a generic walking TC theory it is possible that the low-energy spectrum contains a technidilaton [9], and this may mainly decay into $\gamma\gamma$ [104]. Further analysis can be carried out by taking into consideration contributions from both light PNGBs from the technicolor sector as well as the technidilaton in the context of our model.

VI. CONCLUSIONS

We have considered a model where electroweak symmetry breaking is due to top-seesaw and technicolor dynamics, and which also contains novel matter fields with quantum numbers of SM matter fields. Hence, as an interesting aside, this model serves as an example of a model with a new type of hybrid fourth generation: while the leptons of the fourth generation transform as usual chiral fermions under the weak gauge group, the QCD quarks of the fourth generation transform as vectorlike fermions. We have carried out a full phenomenology analysis of this model and established the spectrum as well as the constraints from the oblique corrections and $Zb\bar{b}$ vertex. We also discussed implications of this model in light of present and future LHC data. In particular, we have showed that the excess in $\gamma\gamma$ channel recently observed at the LHC could be explained as due to decay of a light CP-odd Higgs boson of this model.

Our model can be viewed as a low-energy effective theory for the composite states arising from the strong dynamics underlying the top seesaw and technicolor, together with a hybrid fourth-generation matter. As an explicit microscopic realization, we have considered a consistent extension of MWT.

Several novel features have been uncovered by our analysis. As in the original MWT model, the fourth-generation leptons play an essential role. First, they provide a clear phenomenological signatures, and, second, they enter the precision constraints and are important for the viability of the model. In the present model, which extends the MWT model to account also for the masses of heavy quarks, the SM-like fourth-generation lepton doublet is accompanied by vectorlike fourth generation of QCD quarks. Hence, this model is very different from the usual extensions of the SM with a sequential fourth generation. We determined the plausible mass spectra for this hybrid fourth generation.

The scalar sector is richer than in MWT, since here, in addition to the technicolor compositeness, there are five physical composite Higgs particles which arise due to the dynamical condensates between third- and fourth-generation QCD quarks. We determined the mass spectrum of these new scalars. In addition, there will be additional scalars from the MWT degrees of freedom and also states of higher spin. In this paper, we have taken these to be heavy and decoupled from the low-energy spectrum, and only considered the effect of technicolor through its contribution to the electroweak symmetry breaking condensate.

In light of early data from LHC, strong dynamics remains as a viable explanation as the mechanism of the

electroweak symmetry breaking to be uncovered in further measurements at the LHC. Any technicolor model requires an extension toward the generation of masses for the (B) SM matter fields. Hence, these types of models are likely to receive further attention in the future.

APPENDIX A: THE EW GAUGE INTERACTION OF QUARKS

In the present model, the fourth-generation leptons are chiral representation under the electroweak gauge group. On the other hand, the fourth-generation QCD quarks are in vector representations under the electroweak gauge group. So, the leptons kinetic terms are identical to the ones in the ordinary SM. However, the fourth-generation quark gauge interactions are different from the SM, and we have

$$\mathcal{L}_{\rm cc} = g_2 \sum_{i=1}^{3} \overline{Q_L^{(i)}}\, \gamma^\mu W_\mu Q_L^{(i)}, \tag{A1}$$

$$\begin{aligned}\mathcal{L}_{\rm nc} = {} & \frac{1}{6} g_1 \sum_{i=1}^{3} \overline{Q_L^{(i)}}\, \gamma^\mu B_\mu Q_L^{(i)} \\ & + g_1 \sum_{i=1}^{3} \overline{Q_R^{(i)}}\, \gamma^\mu \begin{pmatrix} 2/3 & 0 \\ 0 & -1/3 \end{pmatrix} B_\mu Q_R^{(i)} \\ & + g_1 \overline{Q^{(4)}} \gamma^\mu \begin{pmatrix} 2/3 & 0 \\ 0 & -1/3 \end{pmatrix} B_\mu Q^{(4)},\end{aligned} \tag{A2}$$

where W_μ (B_μ) are $SU(2)$ ($U(1)$) gauge boson fields, $g_{2(1)}$ is short for the $SU(2)$ ($U(1)_Y$) gauge coupling, and $Q_R^{(i)} = (U_R^{(i)}, D_R^{(i)})^T$. By using the rotation matrix in Eq. (16), these interactions can be represented in terms of the mass basis. The resulting vertices are shown in Table III where $P_{L,R} = (1 \mp \gamma_5)/2$ and the matrices $\mathcal{V}$, $\mathcal{U}$, $\mathcal{D}$ are given by

$$\mathcal{V}_{\alpha\beta} \equiv \sum_{i=1}^{3} U_{i\alpha}^{(L)*} D_{i\beta}^{(L)} = \delta_{\alpha\beta} - U_{4\alpha}^{(L)*} D_{4\beta}^{(L)}, \tag{A3}$$

$$\mathcal{U}^L_{\alpha\beta} \equiv \sum_{i=1}^{3} U_{i\alpha}^{(L)*} U_{i\beta}^{(L)} = \delta_{\alpha\beta} - U_{4\alpha}^{(L)*} U_{4\beta}^{(L)}, \tag{A4}$$

$$\mathcal{D}^L_{\alpha\beta} \equiv \sum_{i=1}^{3} D_{i\alpha}^{(L)*} D_{i\beta}^{(L)} = \delta_{\alpha\beta} - D_{4\alpha}^{(L)*} D_{4\beta}^{(L)}, \tag{A5}$$

which are not necessarily unitary.

APPENDIX B: EFFECTIVE THEORY PARAMETERS

The masses $\mathcal{M}_\pi^2$ and $\mathcal{M}_{\pi^\pm}^2$ in the low-energy effective theory are given in terms of the high-energy theory parameters through the computation of Fig. 2(a) as

$$M_A^2 = \frac{\xi \Lambda^2}{\cos\beta \sin\beta \sqrt{Z_{\Phi_1} Z_{\Phi_2}}}, \tag{B1}$$

where we have dropped $\mathcal{O}(\xi^2)$, and

$$\begin{aligned}M_{H^\pm}^2 = {} & [\mathcal{M}_{\pi^\pm}^2]_{11} \sin^2\beta + [\mathcal{M}_{\pi^\pm}^2]_{22} \cos^2\beta \\ & + 2[\mathcal{M}_{\pi^\pm}^2]_{12} \sin\beta\cos\beta,\end{aligned} \tag{B2}$$

$$\begin{aligned}[\mathcal{M}_{\pi^\pm}^2]_{11} = {} & Z_{\Phi_1}^{-1} \Bigg[\Bigg(1 - \frac{3y_{10}^2}{8\pi^2} \sum_{\alpha,\beta=1}^{4} |D_{\alpha 4}^R|^2 |U_{\beta 3}^L|^2 \Bigg) \Lambda^2 \\ & + \frac{3y_{10}^2}{8\pi^2} \sum_{\alpha,\beta=1}^{4} |D_{\alpha 4}^R|^2 |U_{\beta 3}^L|^2 F_1(m_{d\alpha}, m_{u\beta}) \Bigg],\end{aligned} \tag{B3}$$

$$\begin{aligned}[\mathcal{M}_{\pi^\pm}^2]_{22} = {} & Z_{\Phi_2}^{-1} \Bigg[\Bigg(1 - \frac{3y_{20}^2}{8\pi^2} \sum_{\alpha,\beta=1}^{4} |D_{\alpha 3}^R|^2 |U_{\beta 4}^L|^2 \Bigg) \Lambda^2 \\ & + \frac{3y_{10}^2}{8\pi^2} \sum_{\alpha,\beta=1}^{4} |D_{\alpha 3}^R|^2 |U_{\beta 4}^L|^2 F_1(m_{d\alpha}, m_{u\beta}) \Bigg],\end{aligned} \tag{B4}$$

$$\begin{aligned}[\mathcal{M}_{\pi^\pm}^2]_{12} = {} & \frac{1}{Z_{\Phi_1} Z_{\Phi_2}} \frac{3y_{10} y_{20}}{8\pi^2} \sum_{\alpha,\beta=1}^{4} \mathrm{Re}[(D_{\alpha 3}^L D_{\alpha 4}^{R*}) \\ & \times (U_{\beta 3}^L U_{\beta 4}^{R*})] F_0(m_{d\alpha}, m_{u\beta}).\end{aligned} \tag{B5}$$

Here, $F_{0,1}(m, M)$ are given by

$$F_0(m, M) = mM \Bigg[\frac{m^2}{m^2 - M^2} \ln\frac{\Lambda^2 + m_1^2}{m_1^2} + \frac{M^2}{M^2 - m^2} \ln\frac{\Lambda^2 + M^2}{M^2} \Bigg] \tag{B6}$$

$$= m^2 \Bigg[\ln\frac{\Lambda^2 + m^2}{m^2} - \frac{\Lambda^2}{\Lambda^2 + m^2} \Bigg], \quad (\text{for } m = M), \tag{B7}$$

$$F_1(m^2, M^2) = \frac{m^4}{m^2 - M^2} \ln\frac{\Lambda^2 + m^2}{m^2} + \frac{M^4}{M^2 - m^2} \ln\frac{\Lambda^2 + M^2}{M^2} \tag{B8}$$

$$= m^2\left[2\ln\frac{\Lambda^2+m^2}{m^2} - \frac{\Lambda^2}{\Lambda^2+m^2}\right], \quad (\text{for } m = M). \tag{B9}$$

Similarly, for the quartic couplings $\lambda'_{t,b}$ and $\lambda_{1,2}$ we obtain through the computation of Fig. 2(b) the relations

$$\lambda'_b = \xi\cdot 2\lambda_1\sqrt{\frac{Z_{\Phi_1}}{Z_{\Phi_2}}}, \qquad \lambda'_t = \xi\cdot 2\lambda_2\sqrt{\frac{Z_{\Phi_2}}{Z_{\Phi_1}}}, \tag{B10}$$

and

$$2\lambda_1 v_1^2 = Z_{\Phi_1}^{-1}\left[\left(1-\frac{3y_{10}^2}{8\pi^2}\right)\Lambda^2 + \frac{3y_{10}^2}{8\pi^2}\sum_{\alpha,\beta=1}^{4}\{\mathrm{Re}[(D^L_{\alpha 3}D^{R*}_{\alpha 4})(D^L_{\beta 3}D^{R*}_{\beta 4})]F_0(m_{d\alpha}, m_{d\beta}) + |D^L_{\alpha 3}|^2|D^R_{\beta 4}|^2F_1(m_{d\alpha}, m_{d\beta})\}\right], \tag{B11}$$

$$2\lambda_2 v_2^2 = Z_{\Phi_2}^{-1}\left[\left(1-\frac{3y_{20}^2}{8\pi^2}\right)\Lambda^2 + \frac{3y_{20}^2}{8\pi^2}\sum_{\alpha,\beta=1}^{4}\{\mathrm{Re}[(U^L_{\alpha 3}U^{R*}_{\alpha 4})(U^L_{\beta 3}U^{R*}_{\beta 4})]F_0(m_{u\alpha}, m_{u\beta}) + |U^L_{\alpha 3}|^2|U^R_{\beta 4}|^2F_1(m_{u\alpha}, m_{u\beta})\}\right]. \tag{B12}$$

APPENDIX C: FORMULAS FOR INTEGRALS

We define the following integrals

$$\mathcal{F}_0(q^2, m^2, M^2) = \int_0^1 dz\,\ln R(q^2, m^2, M^2), \tag{C1}$$

$$\mathcal{F}_1(q^2, m^2, M^2) = \int_0^1 dz[R(q^2, m^2, M^2) + z(z-1)q^2]\ln R(q^2, m^2, M^2), \tag{C2}$$

$$\mathcal{F}_2(q^2, m^2, M^2) = \int_0^1 dz R(q^2, m^2, M^2)\ln R(q^2, m^2, M^2), \tag{C3}$$

$$R(q^2, m^2, M^2) = z(z-1)q^2 + (1-z)m^2 + zM^2. \tag{C4}$$

These are evaluated as

$$\mathcal{F}_0(q^2, m^2, M^2) = \frac{1}{2}\ln(xy) - 2 - \frac{f(x,x)+f(y,y)}{4} + \frac{1}{2}\left[\chi_-(x,y) - \frac{1}{2}\theta_-(x,y)\right], \tag{C5}$$

$$\mathcal{F}_0(0, m^2, M^2) = \tfrac{1}{2}\ln(xy) - \tfrac{1}{2}\theta_-(x,y), \tag{C6}$$

$$\mathcal{F}_1(q^2, m^2, M^2) = \frac{5}{9} - \frac{x+y}{3} - \frac{1}{6}\ln(xy) + \frac{x\ln x + y\ln y}{2} - \frac{x-1}{12}f(x,x) - \frac{x-1}{12}f(y,y) + \frac{1}{2}\left[\chi_+(x,y) - \frac{1}{2}\theta_+(x,y)\right], \tag{C7}$$

$$\mathcal{F}_2(q^2, m^2, M^2) = \frac{x\ln x + y\ln y}{2} - \frac{1}{4}\theta_+(x,y) + \mathcal{F}'_1(x,y) + \frac{(x-y)^2-(x+y)}{2}\mathcal{F}'_0(x,y), \tag{C8}$$

$$\mathcal{F}_1(0, m^2, M^2) = \mathcal{F}_2(0, m^2, M^2) = \frac{x\ln x + y\ln y}{2} - \frac{1}{4}\theta_+(x,y), \tag{C9}$$

$$\mathcal{F}'_0(q^2, m^2, M^2) = \mathcal{F}_0(q^2, m^2, M^2) - \mathcal{F}_0(0, m^2, M^2), \tag{C10}$$

$$\mathcal{F}'_1(q^2, m^2, M^2) = \mathcal{F}_1(q^2, m^2, M^2) - \mathcal{F}_1(0, m^2, M^2), \tag{C11}$$

where $\theta_\pm(x,y)$ and $\chi_\pm(x,y)$ are given by [73]

$$\theta_+(x,y) = x + y - \frac{2xy}{x-y}\ln\frac{x}{y}, \tag{C12}$$

$$\theta_-(x,y) = \frac{x+y}{x-y}\ln\frac{x}{y} - 2, \tag{C13}$$

$$\chi_+(x,y) = \frac{x+y}{2} - \frac{(x-y)^2}{3} + \left[\frac{(x-y)^3}{6} - \frac{x^2+y^2}{2(x-y)}\right]\ln\frac{x}{y} \tag{C14}$$

$$\begin{aligned} &+ \frac{x-1}{6}f(x,x) + \frac{x-1}{6}f(y,y) + \left[\frac{1}{3} - \frac{x+y}{6} - \frac{(x-y)^2}{6}\right]f(x,y), \\ \chi_-(x,y) &= 2 + \left[x - y - \frac{x+y}{x-y}\right]\ln\frac{x}{y} + \frac{f(x,x)+f(y,y)}{2} - f(x,y), \end{aligned} \tag{C15}$$

$$\theta_\pm(x,x) = \chi_\pm(x,x) = 0, \tag{C16}$$

$$f(x,y) = \begin{cases} -2\sqrt{\Delta}\left[\arctan\frac{x-y+1}{\sqrt{\Delta}} - \arctan\frac{x-y-1}{\sqrt{\Delta}}\right] & \text{for } \Delta > 0 \\ 0 & \text{for } \Delta = 0 \\ \sqrt{-\Delta}\ln\frac{x+y-1+\sqrt{-\Delta}}{x+y-1-\sqrt{-\Delta}} & \text{for } \Delta < 0, \end{cases} \tag{C17}$$

$$\Delta = -1 + 2(x+y) - (x-y)^2, \tag{C18}$$

in which $\theta_\pm(x,x)$, $\chi_\pm(x,x) = 0$. In this Appendix, x, y are given by

$$x = \begin{cases} \frac{m^2}{q^2} & \text{for } q^2 \neq 0 \\ \frac{m^2}{M_Z^2} & \text{for } q^2 \neq 0, \end{cases} \qquad y = \begin{cases} \frac{M^2}{q^2} & \text{for } q^2 \neq 0 \\ \frac{M^2}{M_Z^2} & \text{for } q^2 \neq 0. \end{cases} \tag{C19}$$

APPENDIX D: DECAY WIDTHS OF THE HIGGS

The decay widths for φ into two gauge bosons are given by

$$\Gamma(\varphi \to gg) = \frac{\alpha_s^2 m_\varphi^3}{32\pi^3 v_{\rm EW}^2}\left|\sum_{i=t,t'} R_i^{(u)}(\varphi)\tau_i A^{(\varphi)}(\tau_i) + \sum_{i=b,b'} R_i^{(d)}(\varphi)\tau_i A^{(\varphi)}(\tau_i)\right|^2, \tag{D1}$$

$$\Gamma(\varphi \to \gamma\gamma) = \frac{\alpha_e^2 m_\varphi^3}{64\pi^3 v_{\rm EW}^2}\left|3\cdot\left(\frac{2}{3}\right)^2\sum_{i=t,t'} R_i^{(u)}(\varphi)\tau_i A^{(\varphi)}(\tau_i) + 3\cdot\left(-\frac{1}{3}\right)^2\sum_{i=b,b'} R_i^{(d)}(\varphi)\tau_i A^{(\varphi)}(\tau_i)\right|^2, \tag{D2}$$

$$\Gamma(h^0 \to WW) = \sin^2(\beta-\alpha)\times\frac{m_h^2}{16\pi v_{\rm EW}^2}\sqrt{1-x_W}\left[1 - x_W + \frac{3}{4}x_W^2\right], \tag{D3}$$

$$\Gamma(h^0 \to ZZ) = \sin^2(\beta-\alpha)\times\frac{m_h^2}{16\pi v_{\rm EW}^2}\sqrt{1-x_Z}\left[1 - x_Z + \frac{3}{4}x_Z^2\right], \tag{D4}$$

where $x_V \equiv 4m_h^2/M_V^2$, $(V = W, Z)$. The decay widths for φ into two fermions are given by

$$\Gamma(\varphi \to t\bar{t}) = [R_3^{(u)}(\varphi)]^2\times\frac{3m_\varphi m_t^2}{8\pi v_{\rm EW}^2}\left[1 - \frac{4m_t^2}{m_\varphi^2}\right]^{1/2}, \tag{D5}$$

$$\Gamma(\varphi \to b\bar{b}) = [R_3^{(d)}(\varphi)]^2\times\frac{3m_\varphi m_b^2}{8\pi v_{\rm EW}^2}\left[1 - \frac{4m_b^2}{m_\varphi^2}\right]^{1/2}, \tag{D6}$$

where $R_i^{(u,d)}(\varphi)$ is given by

$$R_i^{(u)}(\varphi) = \begin{cases} \frac{\Sigma_U}{m_i}[U_{i3}^{L*}U_{i4}^{R}]\frac{1}{\cos\phi}\frac{\cos\alpha}{\sin\beta} & \text{for } \varphi = h \\ \frac{\Sigma_U}{m_i}[U_{i3}^{L*}U_{i4}^{R}]\frac{\cot\beta}{\cos\phi} & \text{for } \varphi = A, \end{cases} \tag{D7}$$

$$R_i^{(d)}(\varphi) = \begin{cases} \frac{\Sigma_D}{m_i}[D_{i3}^{L*}D_{i4}^{R}]\frac{1}{\cos\phi}\frac{\sin\alpha}{\cos\beta} & \text{for } \varphi = h \\ \frac{\Sigma_D}{m_i}[D_{i3}^{L*}D_{i4}^{R}]\frac{\tan\beta}{\cos\phi} & \text{for } \varphi = A, \end{cases} \tag{D8}$$

and $A^{(\varphi)}(\tau_i)$, $(\tau_i \equiv 4m_i^2/m_\varphi^2)$ is given by

$$A^{(\varphi)}(\tau_i) = \begin{cases} 1 + (1-\tau_i)A(\tau_i) & \text{for } \varphi = h \\ A(\tau_i) & \text{for } \varphi = A, \end{cases} \tag{D9}$$

where

$$A(\tau_i) = \begin{cases} [\arcsin(1/\sqrt{\tau_i})]^2 & \text{for } \tau_i > 1 \\ -\frac{1}{4}\left[\log\frac{1+\sqrt{1-\tau_i}}{1-\sqrt{1-\tau_i}} - i\pi\right]^2 & \text{for } \tau_i \le 1. \end{cases} \tag{D10}$$

The above decay widths Eqs. (D1), (D2), (D5), and (D6) are similar as in the two-Higgs-doublet model [102], but taking into account also the fourth-family quarks contributions. In addition, if kinematically allowed, h^0 decays into A^0A^0 and A^0Z^0 and these decay widths are given by

$$\Gamma(h^0 \to A^0A^0) = \frac{\lambda_{hAA}^2}{32\pi m_h}\sqrt{1 - \frac{4m_A^2}{m_h^2}}, \tag{D11}$$

$$\Gamma(h^0 \to A^0Z) = \cos^2(\beta-\alpha) \times \frac{m_h^3}{16\pi v_{\rm EW}^2}\left[1 - \frac{(m_A - M_Z)^2}{m_h^2}\right]^{3/2}\left[1 - \frac{(m_A + M_Z)^2}{m_h^2}\right]^{3/2}, \tag{D12}$$

where λ_{hAA} is represented as

$$\begin{aligned}\lambda_{hAA} = {} & \lambda_b v_1 \sin\alpha\sin^2_\beta - \lambda_t v_2 \cos\alpha\cos^2\beta - \tfrac{1}{2}\lambda_{tb}\sin(\beta-\alpha)[v_1\cos\beta + v_2\sin\beta] \\ & - \tfrac{1}{2}\lambda'_b[(v_1\cos\beta - v_2\sin\beta)\sin\alpha - v_1\sin(\beta-\alpha)\sin\beta] - \tfrac{1}{2}\lambda'_t[(v_1\cos\beta - v_2\sin\beta)\cos\alpha - v_2\sin(\beta+\alpha)\cos\beta],\end{aligned} \tag{D13}$$

and follows from the potential Eq. (25) in the mass eigenbasis for each Higgs boson.

[1] S. Weinberg, Phys. Rev. D **13**, 974 (1976); **19**, 1277 (1979); L. Susskind, Phys. Rev. D **20**, 2619 (1979).
[2] C. T. Hill and E. H. Simmons, Phys. Rep. **381**, 235 (2003); **390**, 553(E) (2004).
[3] F. Sannino, Acta Phys. Pol. B **40**, 3533 (2009) [http://th-www.if.uj.edu.pl/acta/vol40/pdf/v40p3533.pdf].
[4] F. Sannino, arXiv:0804.0182.
[5] M. E. Peskin and T. Takeuchi, Phys. Rev. Lett. **65**, 964 (1990); Phys. Rev. D **46**, 381 (1992).
[6] F. Sannino and K. Tuominen, Phys. Rev. D **71**, 051901 (2005).
[7] D. D. Dietrich, F. Sannino, and K. Tuominen, Phys. Rev. D **72**, 055001 (2005).
[8] B. Holdom, Phys. Lett. **150B**, 301 (1985).
[9] K. Yamawaki, M. Bando, and K. Matumoto, Phys. Rev. Lett. **56**, 1335 (1986).
[10] T. Akiba and T. Yanagida, Phys. Lett. **169B**, 432 (1986).
[11] T. W. Appelquist, D. Karabali, and L. C. R. Wijewardhana, Phys. Rev. Lett. **57**, 957 (1986).
[12] T. Banks and A. Zaks, Nucl. Phys. **B196**, 189 (1982).
[13] S. Catterall and F. Sannino, Phys. Rev. D **76**, 034504 (2007).
[14] A. J. Hietanen, J. Rantaharju, K. Rummukainen, and K. Tuominen, J. High Energy Phys. 05 (2009) 025.
[15] L. Del Debbio, A. Patella, and C. Pica, Phys. Rev. D **81**, 094503 (2010).
[16] A. J. Hietanen, K. Rummukainen, and K. Tuominen, Phys. Rev. D **80**, 094504 (2009).
[17] F. Bursa, L. Del Debbio, L. Keegan, C. Pica, and T. Pickup, Phys. Rev. D **81**, 014505 (2010).
[18] Y. Shamir, B. Svetitsky, and T. DeGrand, Phys. Rev. D **78**, 031502 (2008).
[19] T. DeGrand, Y. Shamir, and B. Svetitsky, Phys. Rev. D **79**, 034501 (2009).

[20] T. DeGrand, Y. Shamir, and B. Svetitsky, Phys. Rev. D **82**, 054503 (2010).
[21] Z. Fodor, K. Holland, J. Kuti, D. Nogradi, and C. Schroeder, J. High Energy Phys. 11 (2009) 103.
[22] J. B. Kogut and D. K. Sinclair, Phys. Rev. D **81**, 114507 (2010).
[23] O. Antipin, M. Heikinheimo, and K. Tuominen, J. High Energy Phys. 07 (2010) 052.
[24] S. Dimopoulos and L. Susskind, Nucl. Phys. **B155**, 237 (1979); E. Eichten and K. D. Lane, Phys. Lett. **90B**, 125 (1980).
[25] T. Appelquist and J. Terning, Phys. Rev. D **50**, 2116 (1994).
[26] T. Appelquist, M. Piai, and R. Shrock, Phys. Rev. D **69**, 015002 (2004).
[27] V. A. Miransky, M. Tanabashi, and K. Yamawaki, Phys. Lett. B **221**, 177 (1989); Mod. Phys. Lett. A **4**, 1043 (1989).
[28] Y. Nambu, Enrico Fermi Institute Report No. 89-08, 1989 (unpublished); in *Proceedings of the 1989 Workshop on Dynamical Symmetry Breaking*, edited by T. Muta and K. Yamawaki (Nagoya University, Nagoya, Japan, 1990).
[29] W. A. Bardeen, C. T. Hill, and M. Lindner, Phys. Rev. D **41**, 1647 (1990).
[30] W. J. Marciano, Phys. Rev. Lett. **62**, 2793 (1989).
[31] C. T. Hill, Phys. Lett. B **266**, 419 (1991); G. Buchalla, G. Burdman, C. T. Hill, and D. Kominis, Phys. Rev. D **53**, 5185 (1996).
[32] C. T. Hill, Phys. Lett. B **345**, 483 (1995).
[33] H. S. Fukano and K. Yamawaki, Prog. Theor. Phys. **119**, 429 (2008).
[34] T. A. Ryttov and R. Shrock, Phys. Rev. D **82**, 055012 (2010).
[35] K. D. Lane and E. Eichten, Phys. Lett. B **222**, 274 (1989).
[36] K. Lane and A. Martin, Phys. Rev. D **80**, 115001 (2009).
[37] A. Delgado, K. Lane, and A. Martin, Phys. Lett. B **696**, 482 (2011).
[38] E. J. Eichten, K. Lane, and A. Martin, Phys. Rev. Lett. **106**, 251803 (2011).
[39] T. Aaltonen *et al.* (CDF Collaboration), Phys. Rev. Lett. **106**, 171801 (2011).
[40] H. S. Fukano and K. Tuominen, arXiv:1102.1254.
[41] B. A. Dobrescu and C. T. Hill, Phys. Rev. Lett. **81**, 2634 (1998).
[42] R. S. Chivukula, B. A. Dobrescu, H. Georgi, and C. T. Hill, Phys. Rev. D **59**, 075003 (1999).
[43] H. J. He, C. T. Hill, and T. M. P. Tait, Phys. Rev. D **65**, 055006 (2002).
[44] P. H. Frampton, P. Q. Hung, and M. Sher, Phys. Rep. **330**, 263 (2000).
[45] H. J. He, N. Polonsky, and S. f. Su, Phys. Rev. D **64**, 053004 (2001).
[46] G. D. Kribs, T. Plehn, M. Spannowsky, and T. M. P. Tait, Phys. Rev. D **76**, 075016 (2007).
[47] M. S. Chanowitz, Phys. Rev. D **79**, 113008 (2009).
[48] J. Erler and P. Langacker, Phys. Rev. Lett. **105**, 031801 (2010).
[49] O. Eberhardt, A. Lenz, and J. Rohrwild, Phys. Rev. D **82**, 095006 (2010).
[50] M. S. Chanowitz, Phys. Rev. D **82**, 035018 (2010).
[51] M. Bobrowski, A. Lenz, J. Riedl, and J. Rohrwild, Phys. Rev. D **79**, 113006 (2009).
[52] A. Soni, A. K. Alok, A. Giri, R. Mohanta, and S. Nandi, Phys. Rev. D **82**, 033009 (2010); Phys. Lett. B **683**, 302 (2010).
[53] A. J. Buras, B. Duling, T. Feldmann, T. Heidsieck, C. Promberger, and S. Recksiegel, J. High Energy Phys. 09 (2010) 106.
[54] A. J. Buras, B. Duling, T. Feldmann, T. Heidsieck, C. Promberger, and S. Recksiegel, J. High Energy Phys. 07 (2010) 094.
[55] A. J. Buras, B. Duling, T. Feldmann, T. Heidsieck, and C. Promberger, J. High Energy Phys. 09 (2010) 104.
[56] L. M. Carpenter, arXiv:1010.5502.
[57] G. Burdman, L. Da Rold, and R. D'E. Matheus, Phys. Rev. D **82**, 055015 (2010).
[58] M. Blennow, E. Fernandez-Martinez, J. Lopez-Pavon, and J. Menendez, J. High Energy Phys. 07 (2010) 096.
[59] S. Antusch, J. P. Baumann, and E. Fernandez-Martinez, Nucl. Phys. **B810**, 369 (2009).
[60] S. Antusch, C. Biggio, E. Fernandez-Martinez, M. B. Gavela, and J. Lopez-Pavon, J. High Energy Phys. 10 (2006) 084.
[61] M. T. Frandsen, I. Masina, and F. Sannino, Phys. Rev. D **81**, 035010 (2010).
[62] A. Lenz, H. Pas, and D. Schalla, Phys. Rev. D **85**, 075025 (2012).
[63] I. Masina and F. Sannino, J. Cosmol. Astropart. Phys. 08 (2011) 018.
[64] B. Holdom, J. High Energy Phys. 08 (2006) 076.
[65] B. Holdom, W. S. Hou, T. Hurth, M. L. Mangano, S. Sultansoy, and G. Unel, PMC Phys. A **3**, 4 (2009).
[66] M. Hashimoto and V. A. Miransky, Phys. Rev. D **81**, 055014 (2010).
[67] M. Hashimoto, Phys. Rev. D **81**, 075023 (2010).
[68] A. Knochel and C. Wetterich, Phys. Lett. B **706**, 320 (2012).
[69] H. E. Haber and R. Hempfling, Phys. Rev. D **48**, 4280 (1993).
[70] R. Foadi, M. T. Frandsen, T. A. Ryttov, and F. Sannino, Phys. Rev. D **76**, 055005 (2007).
[71] R. S. Chivukula, E. H. Simmons, B. Coleppa, H. E. Logan, and A. Martin, Phys. Rev. D **83**, 055013 (2011).
[72] K. Hagiwara, S. Matsumoto, D. Haidt, and C. S. Kim, Z. Phys. C **64**, 559 (1994).
[73] L. Lavoura and J. P. Silva, Phys. Rev. D **47**, 2046 (1993).
[74] T. Appelquist and G. Triantaphyllou, Phys. Lett. B **278**, 345 (1992).
[75] R. Sundrum and S. D. H. Hsu, Nucl. Phys. **B391**, 127 (1993).
[76] M. Harada and Y. Yoshida, Phys. Rev. D **50**, 6902 (1994).
[77] T. Appelquist and F. Sannino, Phys. Rev. D **59**, 067702 (1999).
[78] S. R. Ignjatovic, L. C. R. Wijewardhana, and T. Takeuchi, Phys. Rev. D **61**, 056006 (2000).
[79] M. Harada, M. Kurachi, and K. Yamawaki, Prog. Theor. Phys. **115**, 765 (2006).
[80] M. Kurachi and R. Shrock, Phys. Rev. D **74**, 056003 (2006).
[81] K. Haba, S. Matsuzaki, and K. Yamawaki, Prog. Theor. Phys. **120**, 691 (2008).
[82] R. S. Chivukula, B. A. Dobrescu, and J. Terning, Phys. Lett. B **353**, 289 (1995).

[83] T. Aaltonen *et al.* (CDF Collaboration), Phys. Rev. D **83**, 112003 (2011).
[84] Y. Bai, J. L. Hewett, J. Kaplan, and T. G. Rizzo, J. High Energy Phys. 03 (2011) 003.
[85] K. Nakamura *et al.* (Particle Data Group Collaboration), J. Phys. G **37**, 075021 (2010).
[86] D. Ludwig for Gfitter Group Collaboration, Proc. Sci., ICHEP2010 (2010) 404 [arXiv:1010.5678].
[87] H. E. Haber and H. E. Logan, Phys. Rev. D **62**, 015011 (2000).
[88] M. Baak *et al.*, arXiv:1107.0975.
[89] W. F. L. Hollik, Fortschr. Phys. **38**, 165 (1990).
[90] H. S. Fukano and K. Tuominen, arXiv:1110.5248.
[91] H. S. Fukano and K. Tuominen, arXiv:1112.0963.
[92] G. Aad *et al.* (ATLAS Collaboration), Phys. Lett. B **708**, 37 (2012).
[93] CMS Collaboration, Report No. CMS PAS EXO-11-050.
[94] CMS Collaboration, Report No. CMS PAS EXO-11-051.
[95] S. Chatrchyan *et al.* (CMS Collaboration), Phys. Lett. B **701**, 204 (2011).
[96] ATLAS Collaboration, Report No. ATLAS-CONF-2011-161.
[97] CMS Collaboration, Report No. CMS-PAS-HIG-11-030.
[98] G. Aad *et al.* (ATLAS Collaboration), Phys. Rev. Lett. **107**, 231801 (2011).
[99] CMS Collaboration, Report No. CMS PAS EXO-11-024.
[100] ATLAS Collaboration, Phys. Lett. B **710**, 383 (2012).
[101] CMS Collaboration, Report No. CMS PAS EXO-11-025.
[102] J. F. Gunion, H. E. Haber, G. L. Kane, and S. Dawson, Front. Phys. **80**, 1 (2000).
[103] S. Dittmaier, C. Mariotti, G. Passarino, R. Tanaka, S. Alekhin, J. Alwall, E. A. Bagnaschi *et al.* (LHC Higgs Cross Section Working Group), arXiv:1201.3084.
[104] S. Matsuzaki and K. Yamawaki, Phys. Rev. D **85**, 095020 (2012).